ATLANTIC
SCIENCE CORPORATION

NASA CR-132823

Scientific Research
Scientific Consultation
Computer Services

(NASA-CR-132823) TRACKING DATA RELAY SATELLITE SYSTEM (TDRSS) VHF PROPAGATION STUDY (Atlantic Science Corp., Indialantic, Fla.) 53 p HC $4.75

N74-10144

CSCL 20N G3/07

Unclas
20268

GENERAL OFFICE: 1701 North A1A • Indialantic, Florida 32903 • Telephone: 305/723-8779
BRANCH OFFICE: P.O. Box 636 • Seabrook, Maryland 20801 • Telephone: 301/459-1692

TRACKING DATA RELAY SATELLITE SYSTEM (TDRSS) VHF PROPAGATION STUDY

TRACKING DATA RELAY SATELLITE SYSTEM (TDRSS) VHF PROPAGATION STUDY

Prepared By:

Lee Ann H. Schleicher
Sigrid K. Llewellyn
Rodney B. Bent

Atlantic Science Corporation
P. O. Box 3201
Indialantic, Florida 32903

Sub-Contracted From:

DBA Systems, Inc.
Melbourne, Florida 32901

Funded By:

National Aeronautics and Space Administration
Goddard Space Flight Center

Contract NAS5-21725

June 15, 1973

//

1.0 INTRODUCTION

This report documents a study performed to investigate the use of the Bent Ionospheric Model in computing corrections to the range and range rate measurements of the TDRSS satellites. Several interesting orbital configurations between the two satellites are discussed as to their effects on total electron content along the radio path between the satellites. Problem areas in the accurate computation of total electron content and range rate corrections are also discussed.

The Bent Ionospheric Model gives the electron density versus height profile as a function of latitude, longitude, height, time, season, and solar flux. In order to explain how this model was used for this study, let us consider Figure 1.

In this figure we see a fixed TDR satellite receiving data from satellite A and satellite B, both immersed in the ionosphere. Considering first satellite A, it is possible from the ephemeris tapes to obtain the ground path of the ray and the height at each known latitude and longitude. With these values, and with the solar information, the ionospheric model will give a value of electron density at each point x, y, z, etc. This data can then be plotted to show the electron density versus distance profile between the two satellites. Figure 2a illustrates the case for satellite A. In the case of satellite B the ray stays within the ionosphere all the time after entering and therefore the N, d profile will be similar to that shown in Figure 2b.

A further advantage of the Bent model is that the maximum height of the ionospheric layer is modeled. Referring again to Figure 1, it is possible to imagine the ray from TDRS to satellite B running along the height of maximum electron density for some time. This is likely because of the rapid changes in $h_m F2$ over short distances. Such a condition could cause considerable errors in total electron content as well as significant angular refraction along the ray.

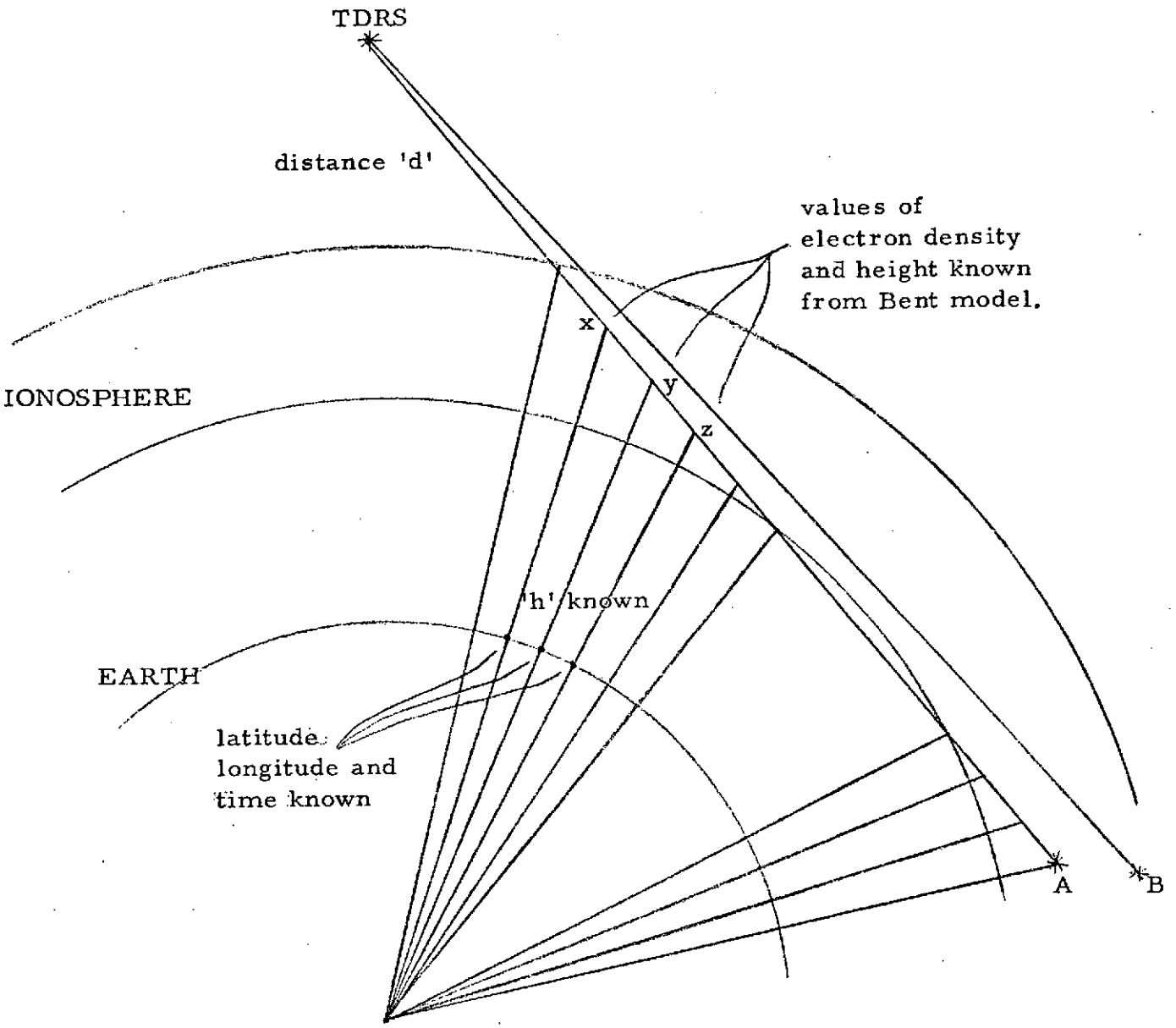
TDRS
distance 'd'
values of
electron density
and height known
from Bent model.
x
y
z
IONOSPHERE
'h' known
EARTH
latitude
longitude and
time known
A
B

Figure 1

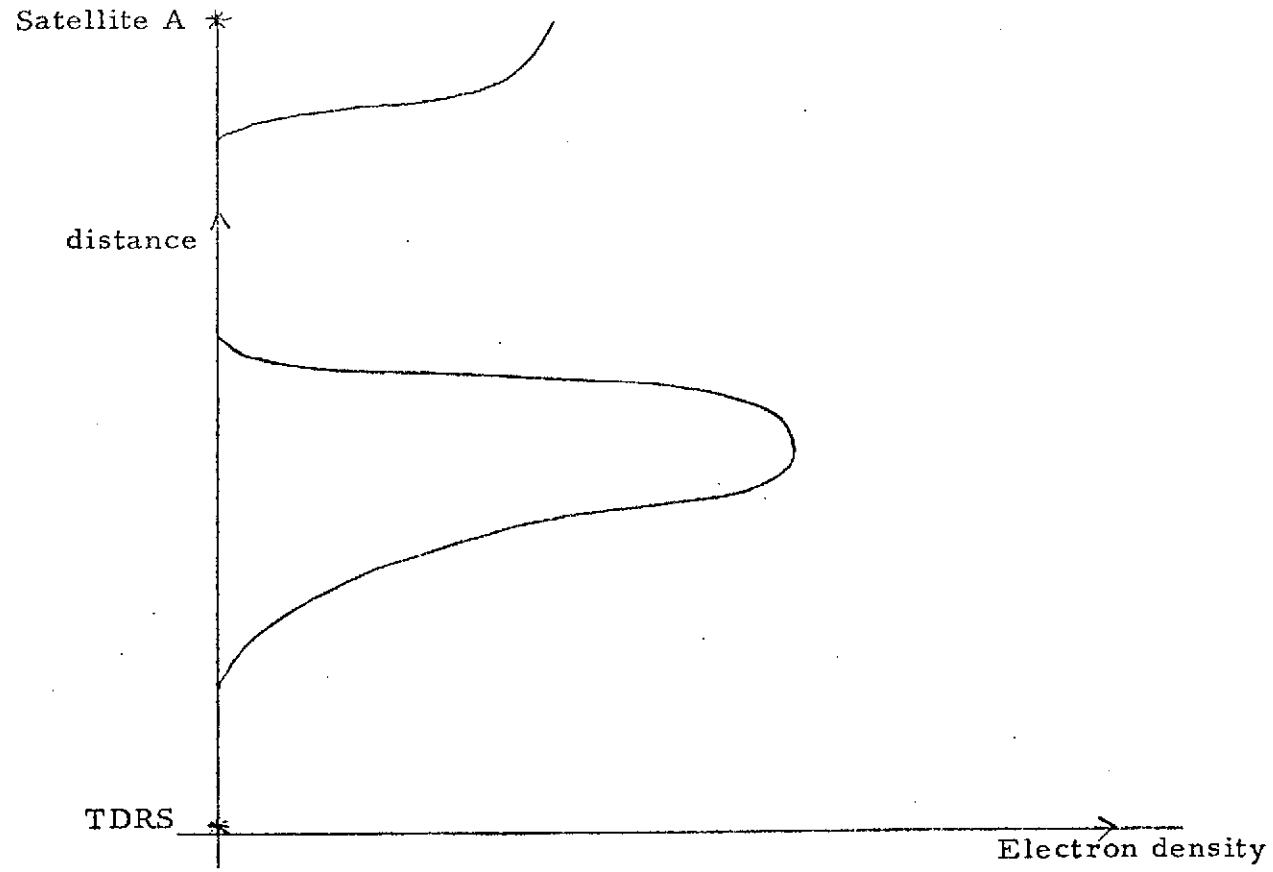

Figure 2a

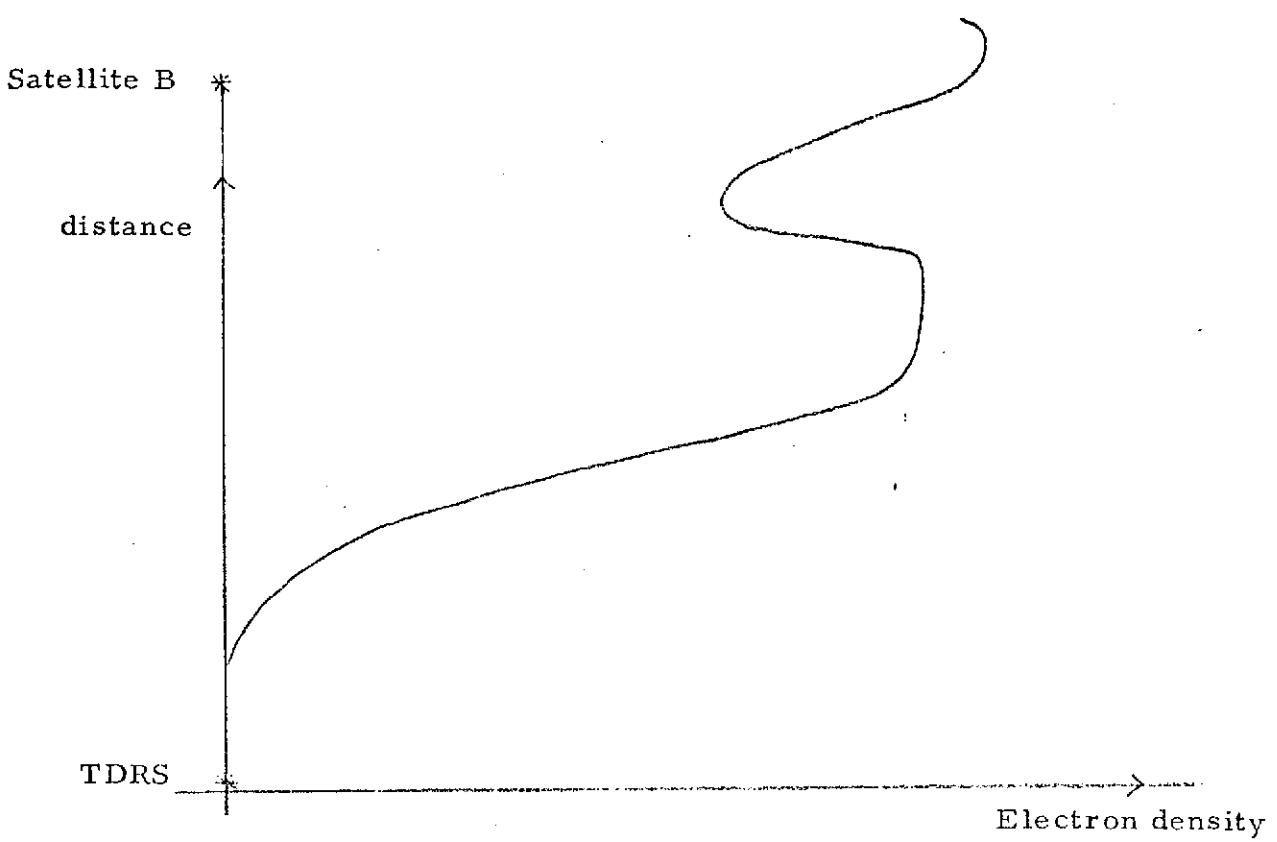

Figure 2b

2.0 RANGE CORRECTIONS

Positional information for a number of satellite orbits was supplied by the National Aeronautics and Space Administration at various heights and inclinations: equatorial, polar, and 30 degree inclinations and 1000, 200, and 350 kilometer heights. Specific cases were chosen from this set of orbits which would best show various effects of looking through parts of the ionosphere with rapidly changing characteristics such as the equatorial anomaly and sunrise effect. The date of the investigation was set at March 15, 1970, a day of average solar activity at the peak of the solar cycle. Although these cases were chosen to investigate the extreme ionospheric refraction situations, the maximum values were probably even larger. The corrections could therefore be still greater than those covered in the following discussion and might be as high as 2×10^{19} e/m^2 column.

It appears that a slight shift in the position of the low satellite may make the difference in whether the ray between the two satellites rides along the height of the maximum electron density (h_m) for long distances or whether the ray hits the maximum at two separated points or whether the ray passes through the ionosphere just above h_m. These slight shifts are likely to make enormous differences in total electron content, which emphasizes the need for an accurate ionospheric profile of electron density versus height.

Three types of graphs will be used in describing the results of running the test conditions through the ionospheric program developed for the TDRSS studies. The first type of graph shows the surface trace of the orbit of the low satellite and the position of the high satellite projected onto the earth's surface. This graph also shows the gradients of $f_x F2$ present at the time given. The second type of graph gives the earth central angles and azimuth angles between the low and high satellites at various points along the orbit

of the low satellite. Azimuth is measured from the high satellite subsatellite point to the low satellite subsatellite point, clockwise from north. The third type of graph shows the total electron content between the satellites calculated for each point along the orbit as well as the minimum height along the path from the low to the high satellite. The minimum height is the point along the ray between the low and high satellite that is closest to the earth.

Figures 3 through 5 are the graphs for Case 1. In Case 1 the low satellite is 1,000 km high and as the low satellite appears over the horizon, the ray between low and high satellite moves along the equatorial anomaly in a horizontal direction. The ray passes through the ionosphere at two different locations. As a result of these conditions, the electron content is very high. When the low satellite passes under the high satellite, the electron content becomes very low since the low satellite is above the ionosphere looking up. As the low satellite gets close to the horizon, it again looks through two ionospheres at the high satellite. This time the electron content is not as high as it was when the low satellite first appeared because the ray is not now passing through the equatorial anomaly.

Figures 6 through 8 describe the results for Case 2. Case 2 is similar to Case 1 except the low satellite is below the ionosphere at a height of 200 kilometers. The ray from the low to the high satellite always passes through one ionosphere, but never through two; hence the peaks in electron content are not as high as they were for Case 1 and when the low satellite moves under the high satellite, the electron content is higher than in Case 1. The electron content is higher as the low satellite appears above the horizon than just before it disappears because, as in Case 1, when it appears above the horizon it is looking through the equatorial anomaly at the high satellite.

Case 3 and Case 4 together demonstrate the sunrise effect. The graphs for Case 3 appear in Figures 9 through 11. In Case 3, the low satellite is

at a height of 1,000 kilometers. In this case the low satellite is looking through a thin ionosphere just before sunrise. The high spike in the plot of electron content just before the low satellite disappears over the horizon is due to the low satellite looking at the high satellite through two ionospheres within the equatorial anomaly belt. Case 4 (Figures 12 through 14) is identical to Case 3 except it occurs 4 hours later. As the low satellite appears over the horizon, it is looking at the high satellite through an ionosphere that has been thickened by the sunrise. The electron content is more than six times higher than it was in Case 3 when the low satellite looks through the sunrise zone. These two cases demonstrate that ionospheric corrections could change very rapidly in a short period of time.

Figures 15 through 17 are plots of the conditions and results for Case 5. The low satellite is at a height of 1,000 kilometers and is in a polar orbit. The high satellite is offset from the orbital plane by approximately 111 degrees. The ray from the low to the high satellite passes through the equatorial anomaly in two different sectors of this orbit. The low satellite is always visible from the high satellite, but only those points where the ray from the low to the high satellite penetrates a significant portion of the ionosphere are considered. Consequently, for most of the points plotted the high satellite is close to the horizon moving almost north and south.

The two peaks in the electron content curve correspond to the portions of the orbit where the low satellite is looking through the equatorial anomaly on both sides of the magnetic equator. When the low satellite is near the geographic equator, there are long periods when the ray from the low to the high satellite penetrates two ionospheres possibly giving higher total content. However, several of these satellite to satellite ray paths ride along the maximum for distances of up to 400 kilometers giving considerable increase in total electron content. The f_0 F2's of the two ionospheres along the ray path are similar because the gradients of the equatorial anomaly do not change rapidly in a horizontal direction.

The graphs for Case 6 are displayed in Figures 18 through 20. In this example the low satellite is in a polar orbit at a height of 200 kilometers. The high satellite is perpendicular to the plane of the orbit and therefore always visible. During the first part of the orbit, the low satellite looks through the thin ionosphere just before sunrise toward the high satellite. The electron content during this part of the orbit is therefore small; however, during the second part of the orbit the low satellite is looking through the equatorial anomaly and the expected double bump in the total electron content curve may be seen. This double bump is similar to that seen in Case 5, but is smaller in magnitude since the low satellite can only look through one ionosphere.

In Case 7 the low satellite is orbiting at a height of 350 kilometers and an inclination of 30 degrees. The graphs for this case are in Figures 21 through 23. The ray from the high to the low satellite rides along h_m for considerable distances and also passes through two ionospheres. For two consecutive sections of 170 kilometers in both ionospheres the ray rides along the maximum for a total of 340 kilometers. The two peaks in the electron content curve capture the effect of the equatorial anomaly. The smaller peak is a result of the low satellite looking through an ionosphere of medium thickness. Between the peaks, however, the satellite is still looking through a dense ionosphere.

The 7 cases just discussed will give the reader a good idea of the various effects on electron content that may result from the use of different orbits and geometrical arrangements of satellites. It is evident that a very accurate electron density model must be used in order to achieve meaningful results, the model being accurate in terms of both electron density and height.

Table 1 is a list for convenient conversion from vertical electron content to range correction for a transmission frequency of 140 MHz,

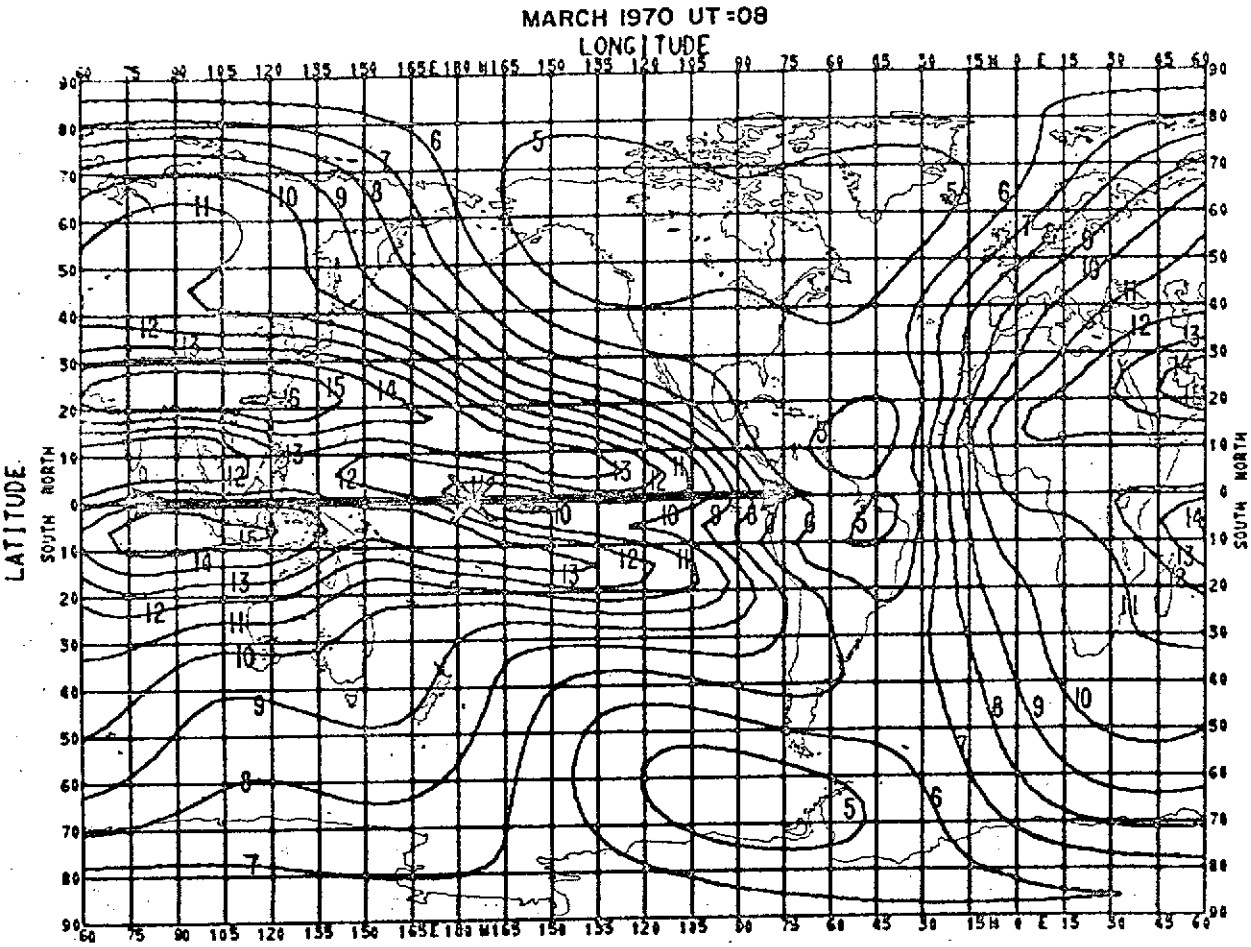

Figure 3

Case 1: Predicted global status of the monthly median f_x F2 showing the stationary high satellite position (X) and the low satellite equatorial orbit (→) at 1000 km.

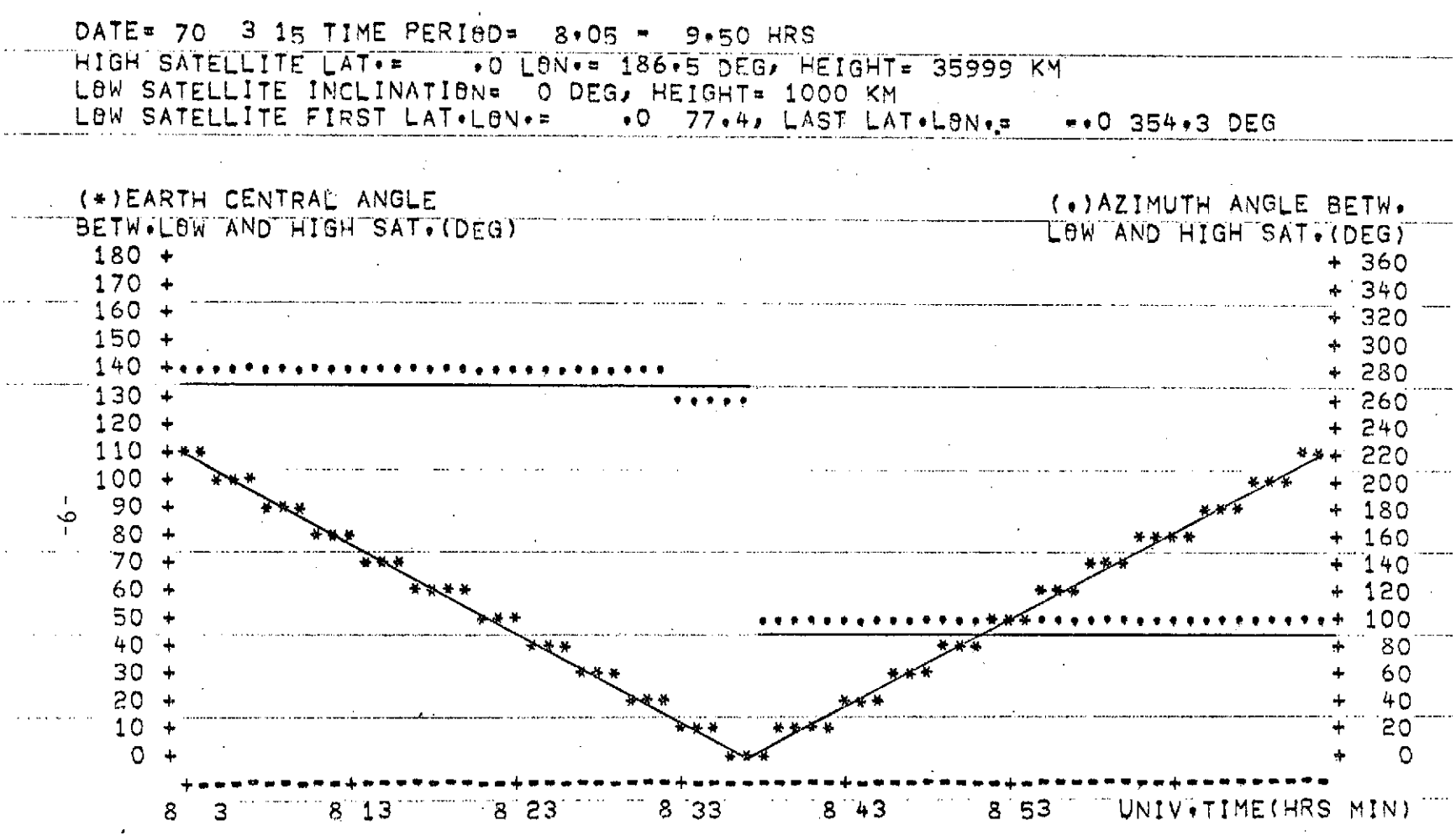

Figure 4

Case 1

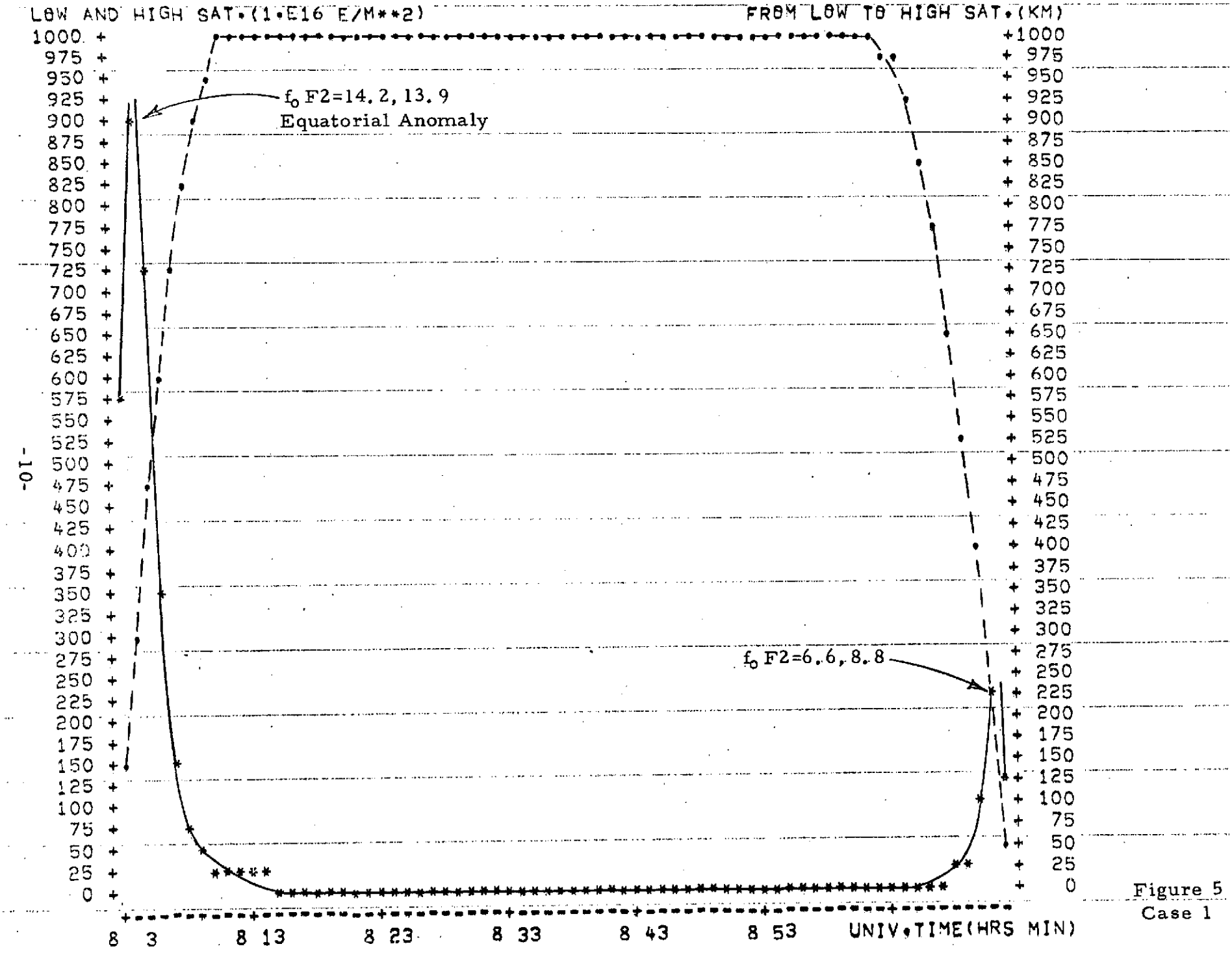

Figure 5
Case 1

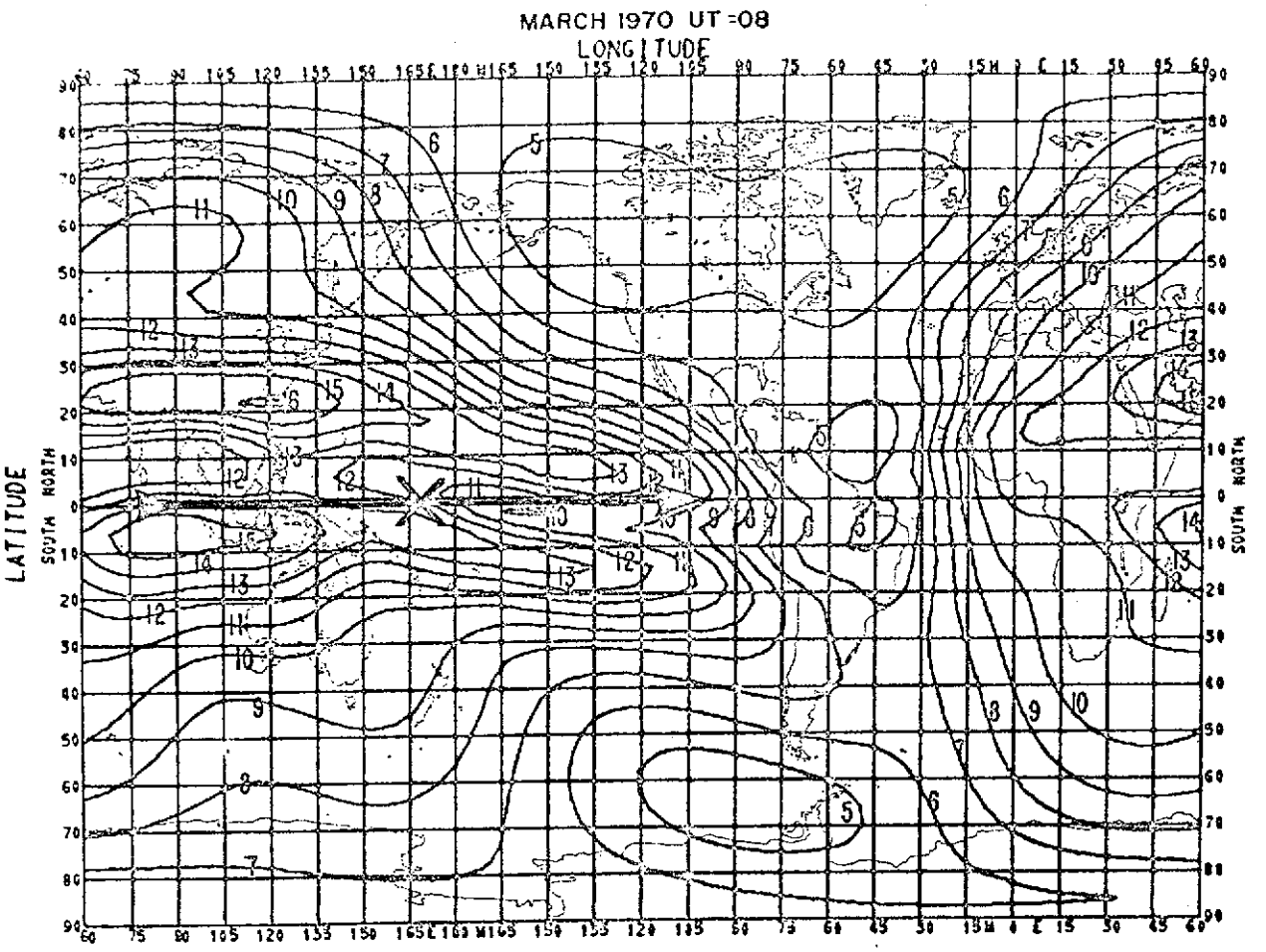

Figure 6

Case 2: Predicted global status of the monthly median f_x F2 showing the stationary high satellite position (X) and the low satellite equatorial orbit (→) at 200 km.

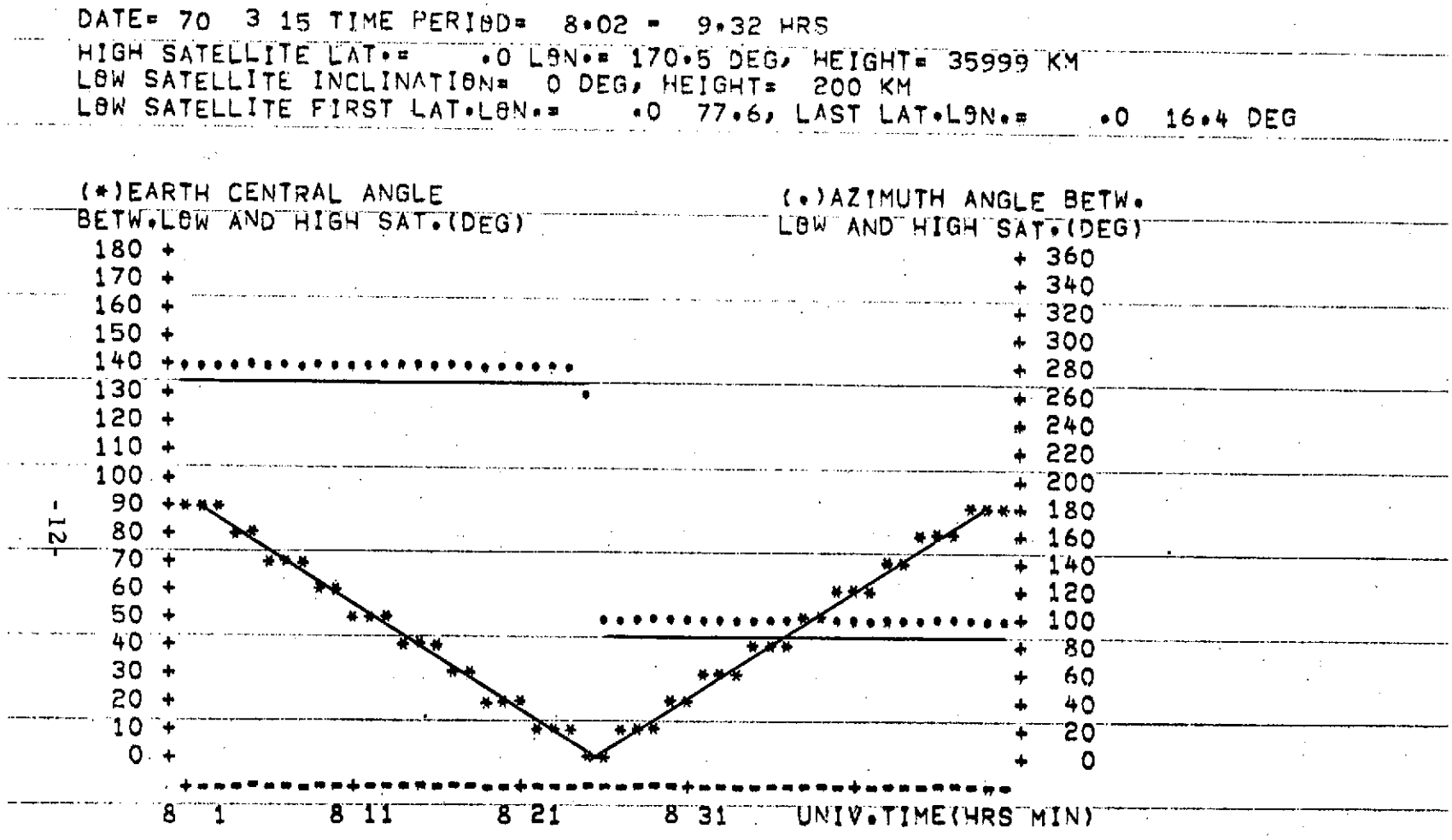

Figure 7

Case 2

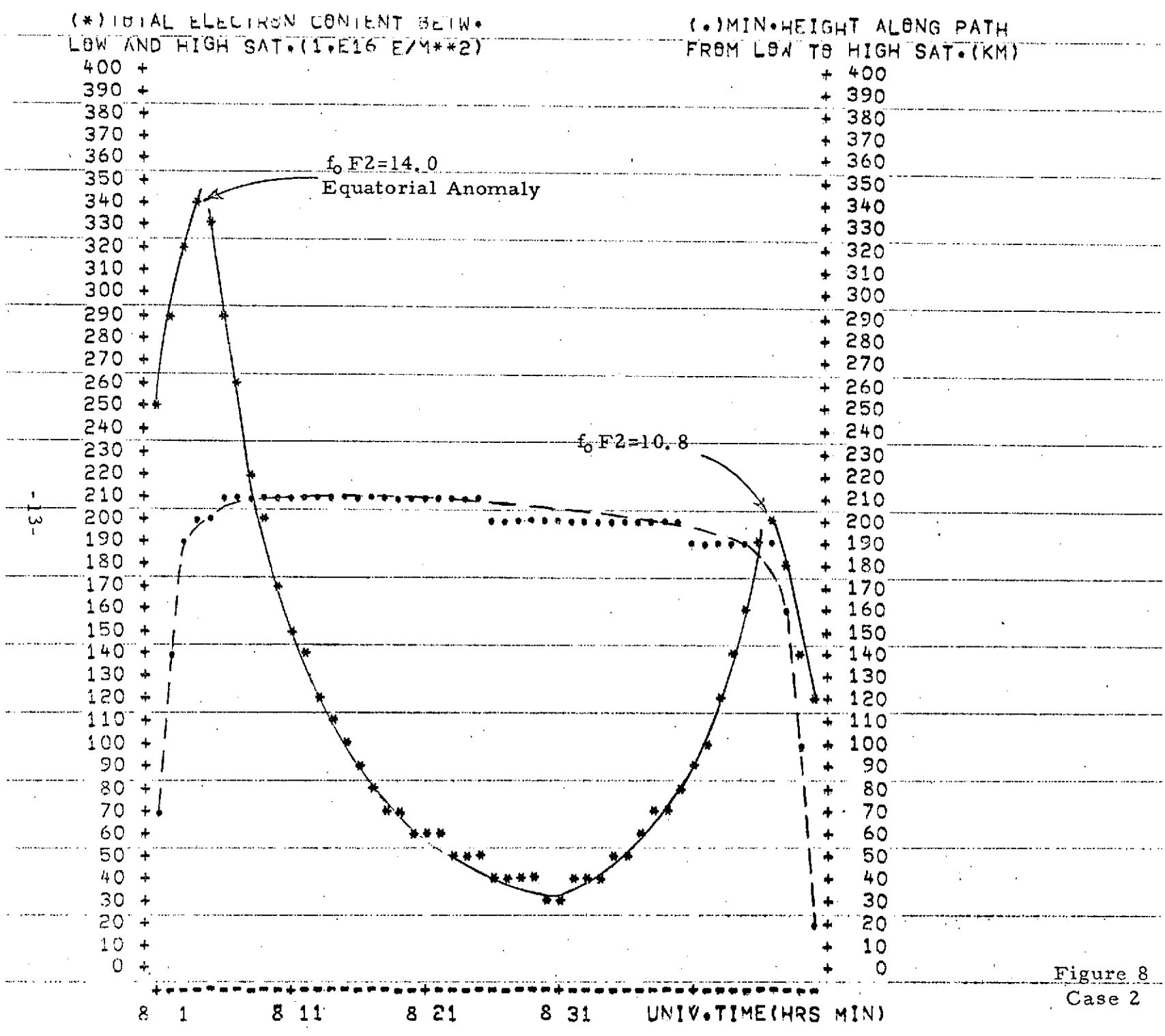

Figure 8
Case 2

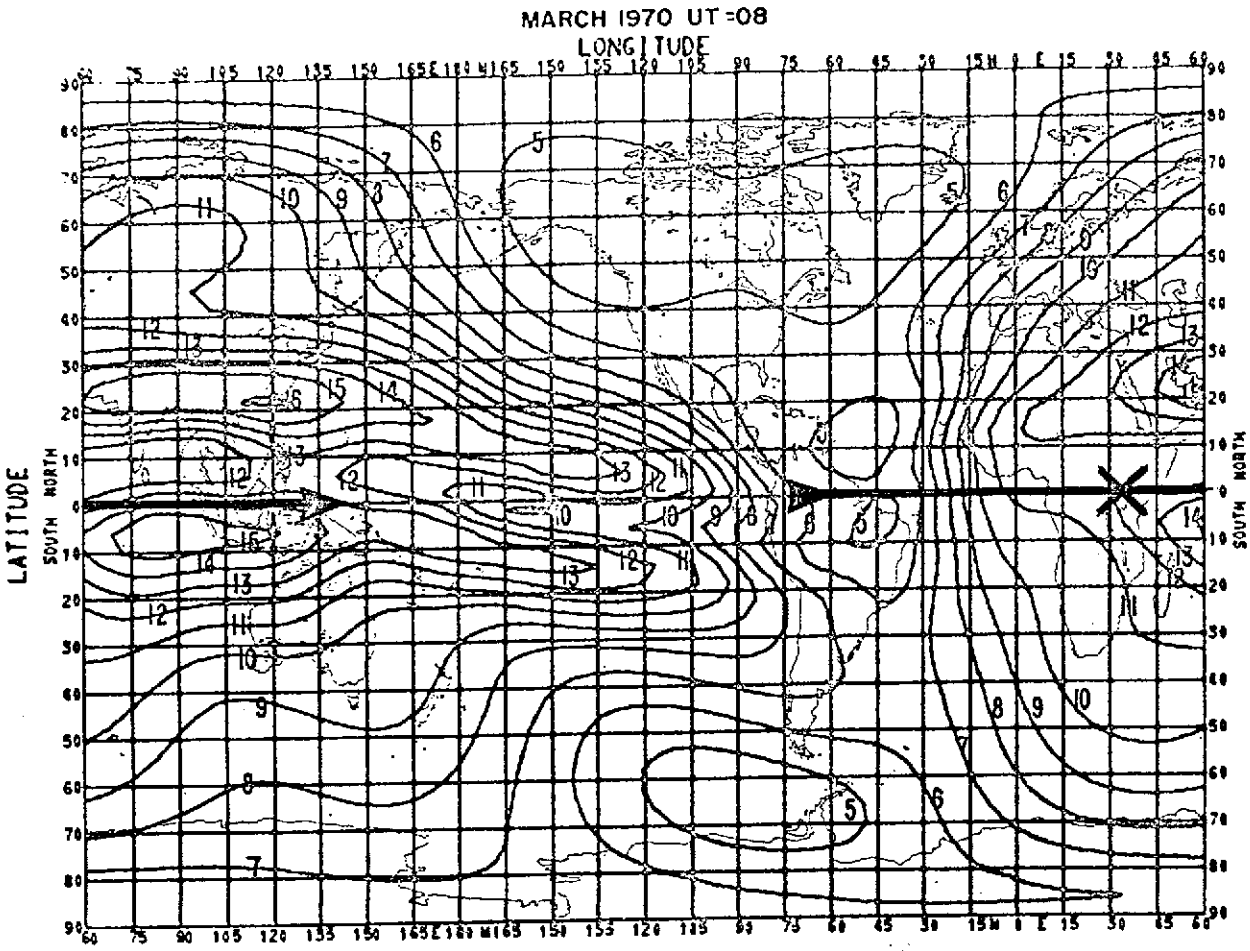

Figure 9

Case 3: Predicted global status of the monthly median f_x F2 showing the stationary high satellite position (X) and the low satellite equatorial orbit (→) at 1000 km.

DATE= 70 3 15 TIME PERIOD= 8.03 - 9.50 HRS
HIGH SATELLITE LAT.= .0 LON.= 36.5 DEG, HEIGHT= 35999 KM
LOW SATELLITE INCLINATION= 0 DEG, HEIGHT= 1000 KM
LOW SATELLITE FIRST LAT.LON.= -.0 287.6, LAST LAT.LON.= -.0 207.6 DEG

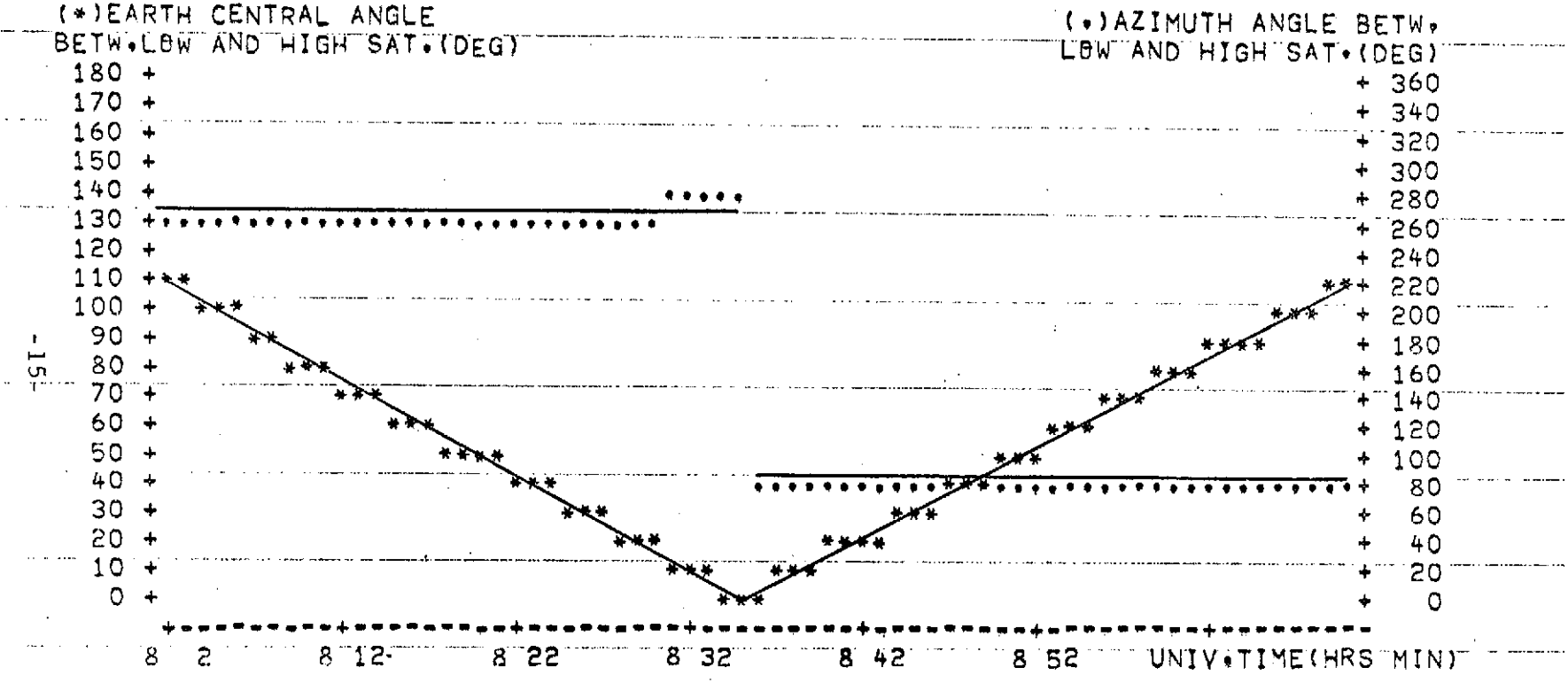

Figure 10

Case 3

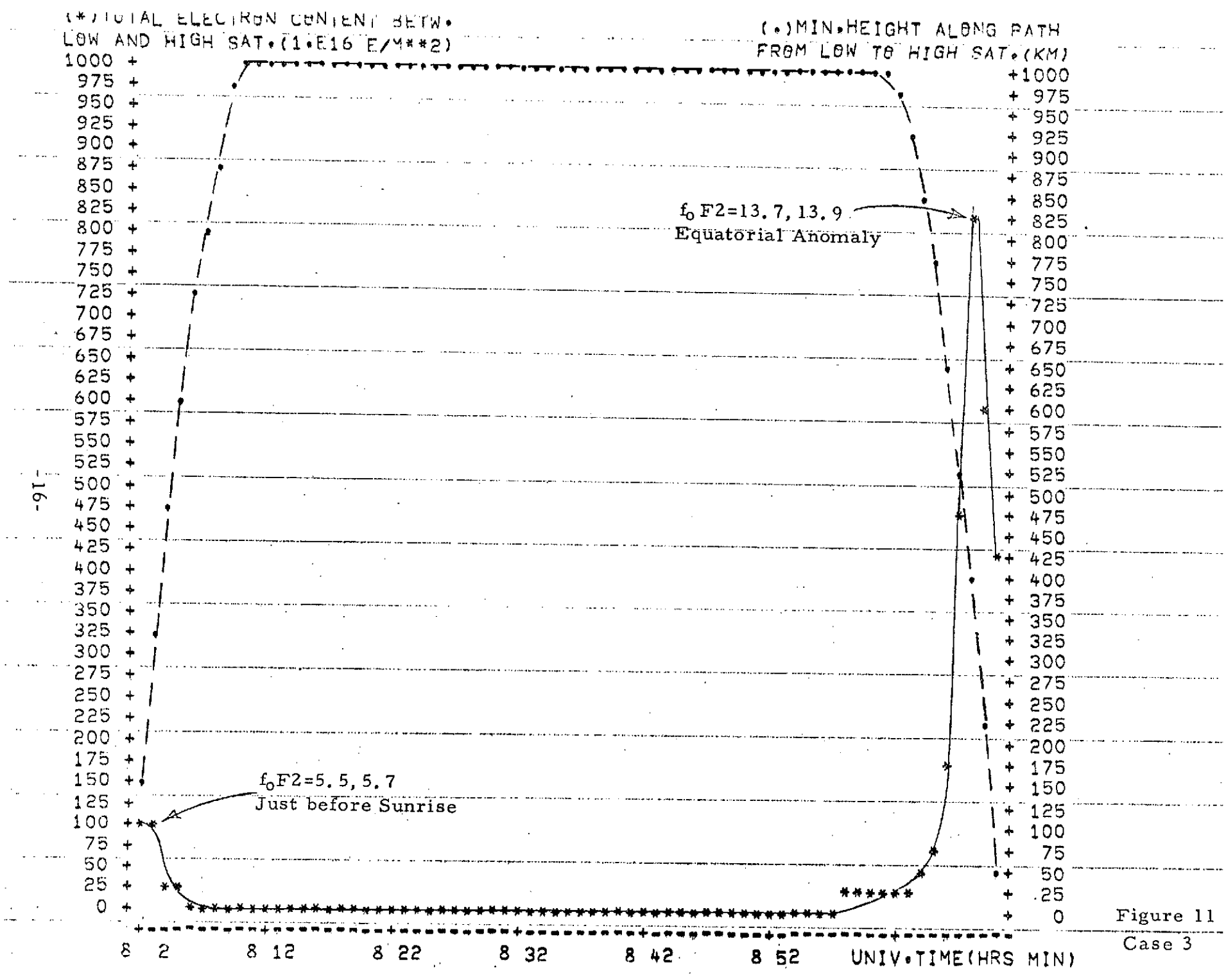

Figure 11
Case 3

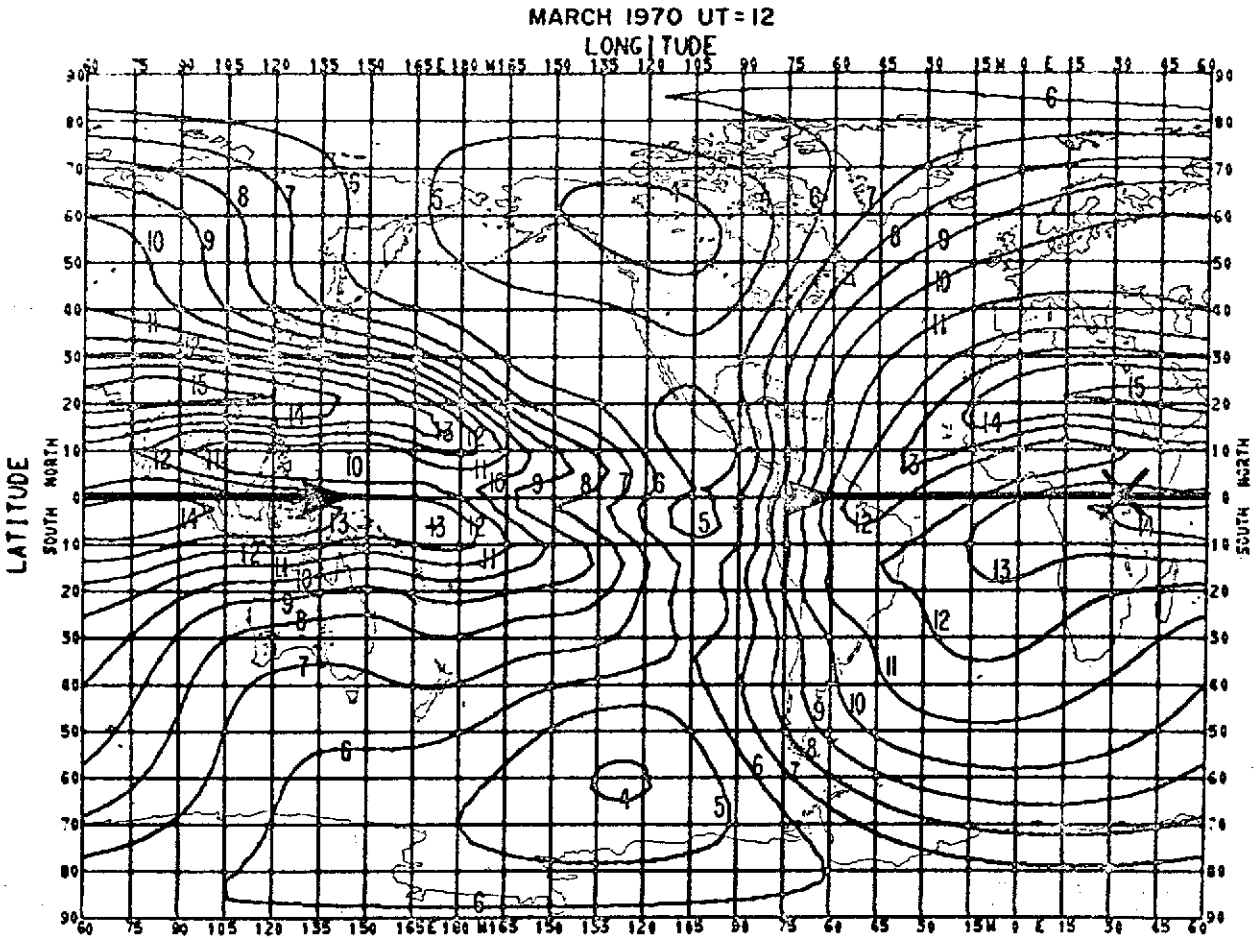

Figure 12

Case 4: Predicted global status of the monthly median f_x F2 showing the stationary high satellite position (X) and the low satellite equatorial orbit (→) at 1000 km.

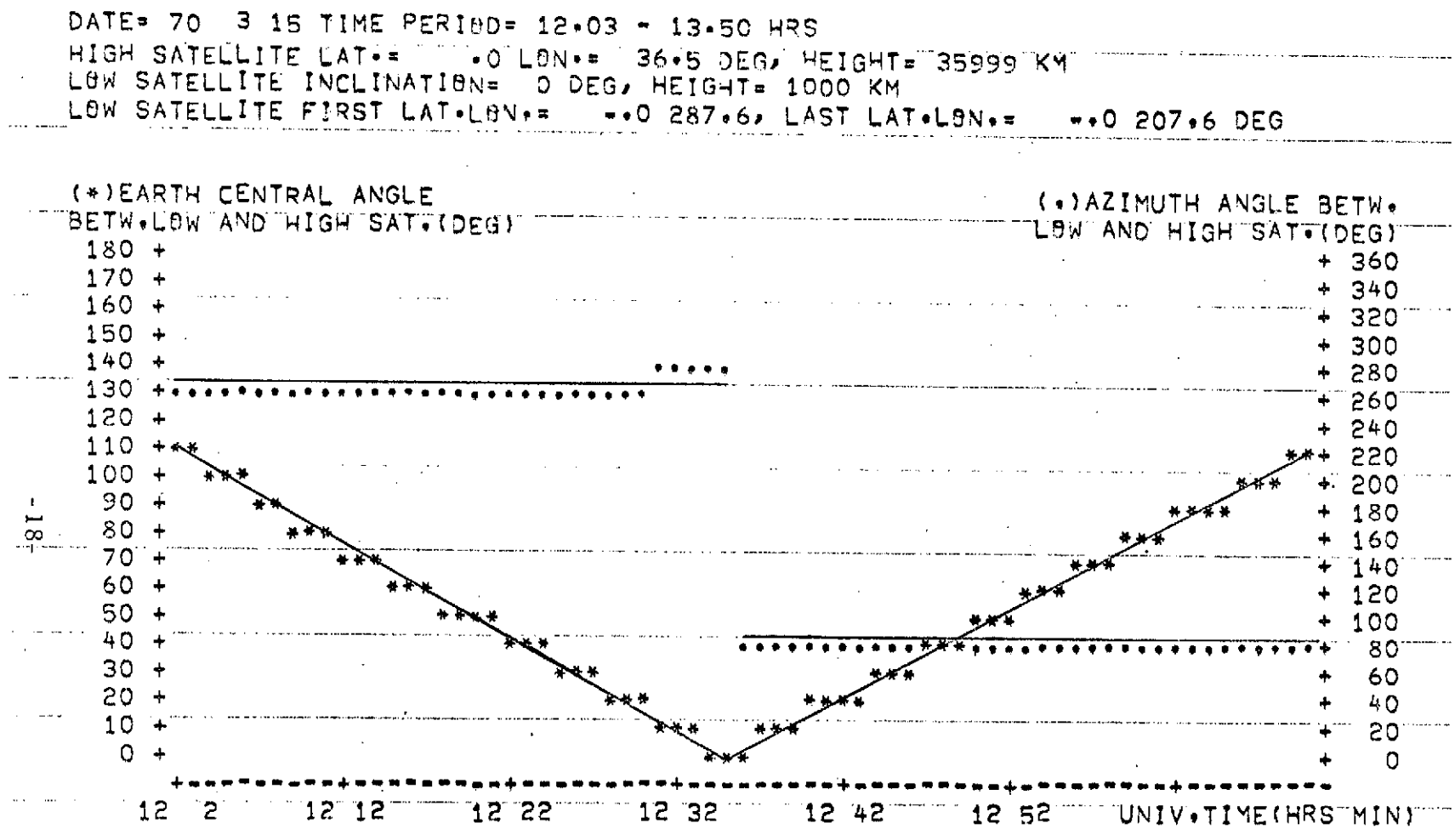

Figure 13
Case 4

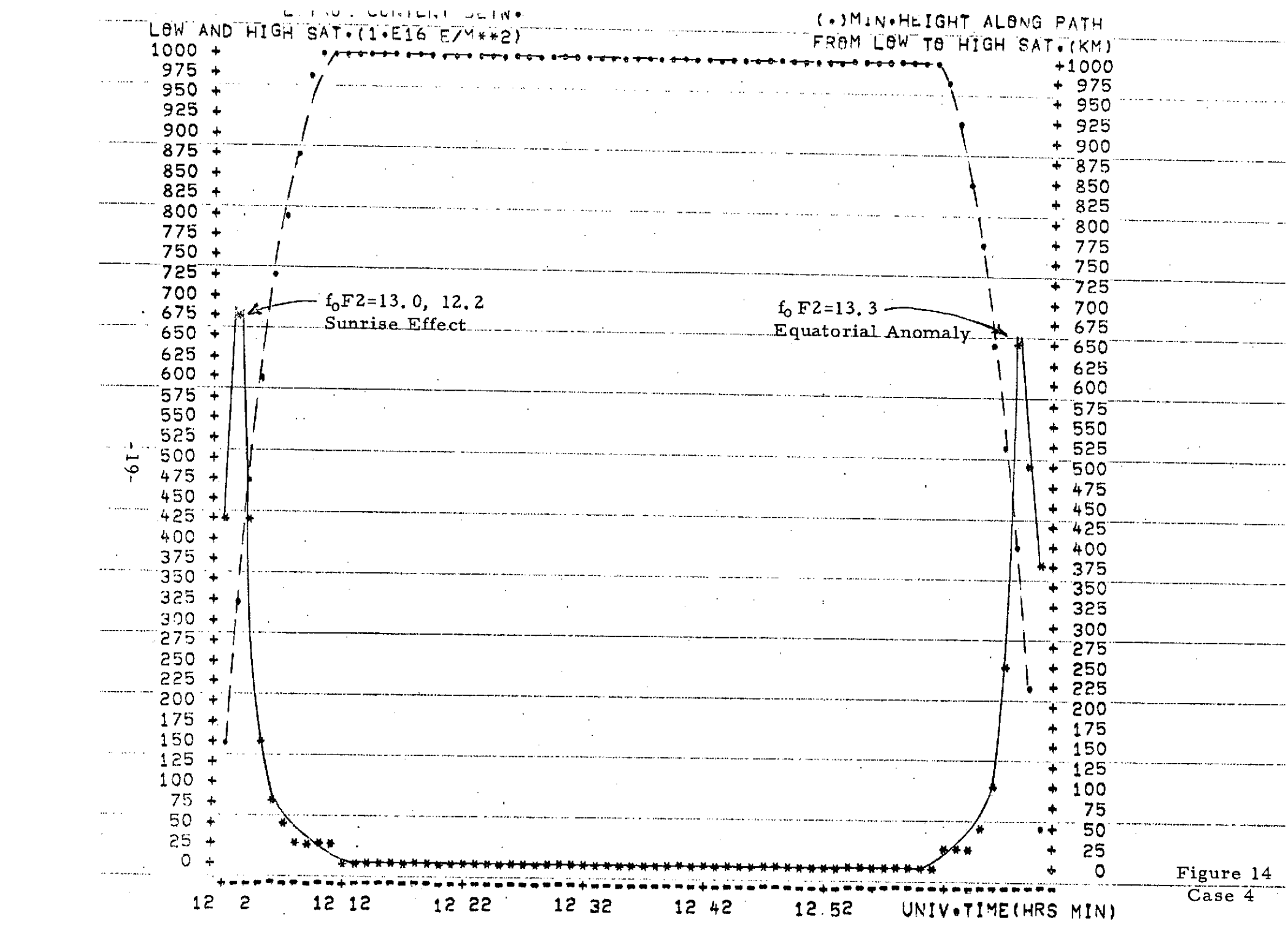

Figure 14
Case 4

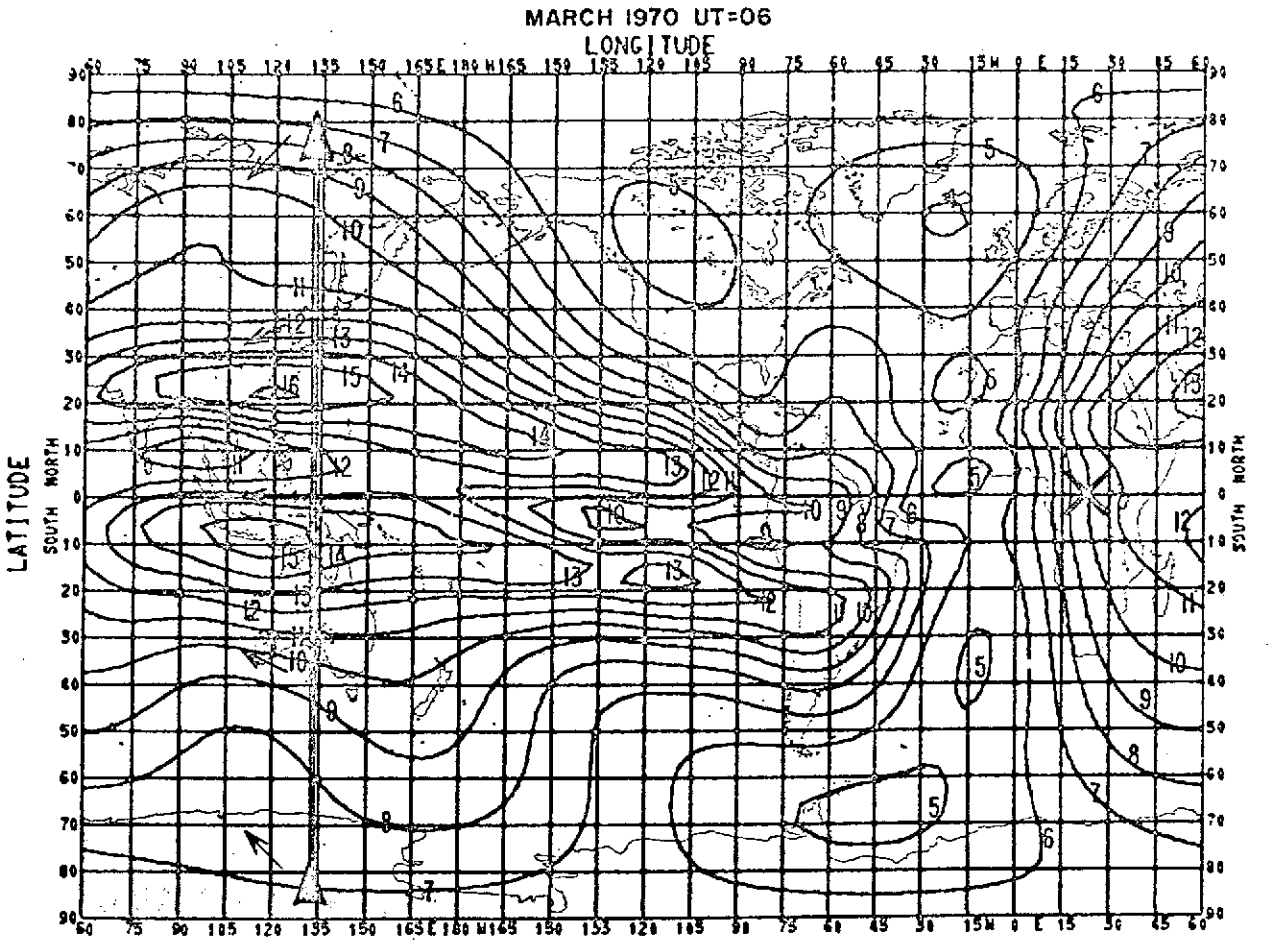

Figure 15

Case 5: Predicted global status of the monthly median f_xF2 showing the stationary high satellite position (X) and the low satellite polar orbit (→) at 1000 km.

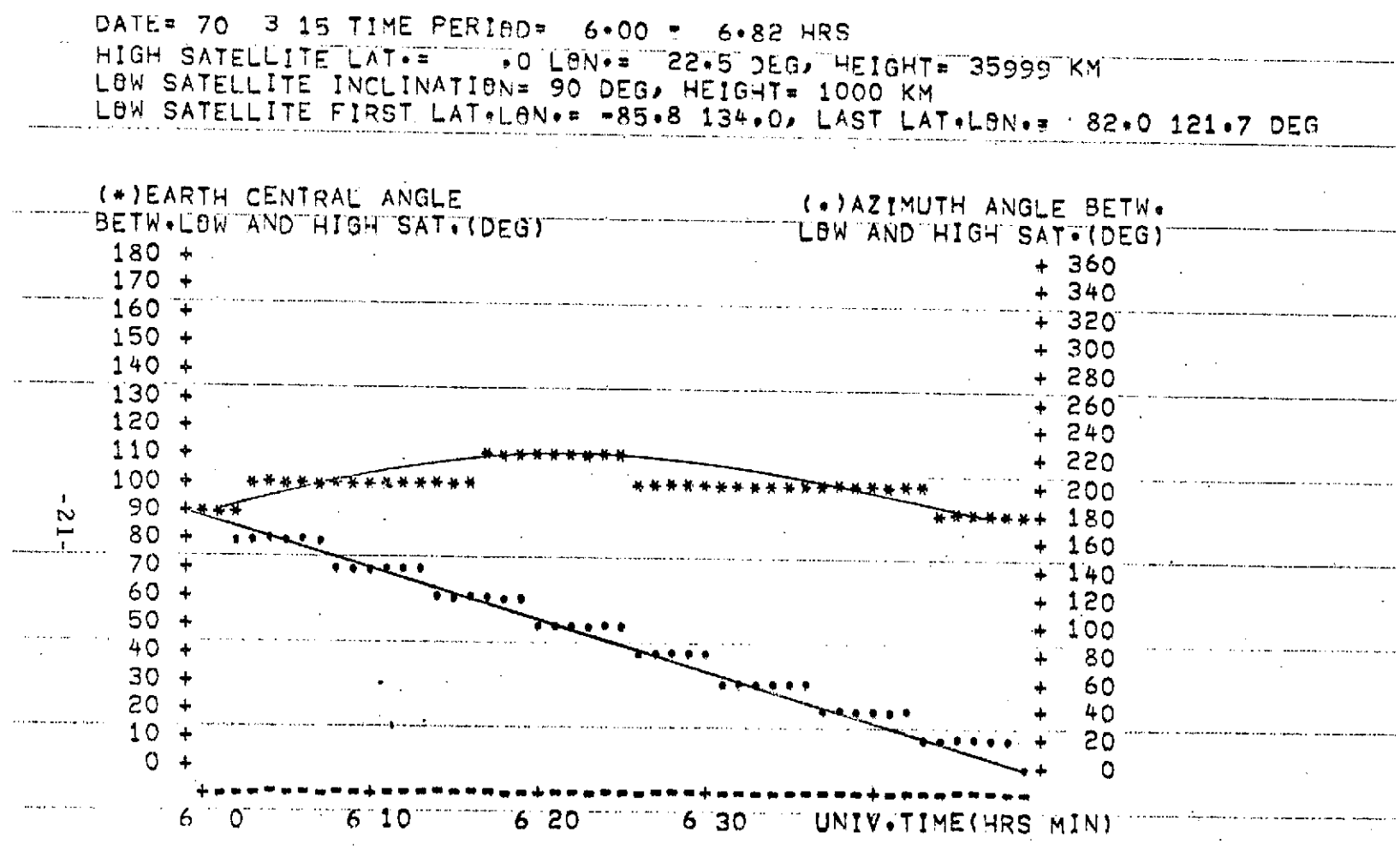

Figure 16

Case 5

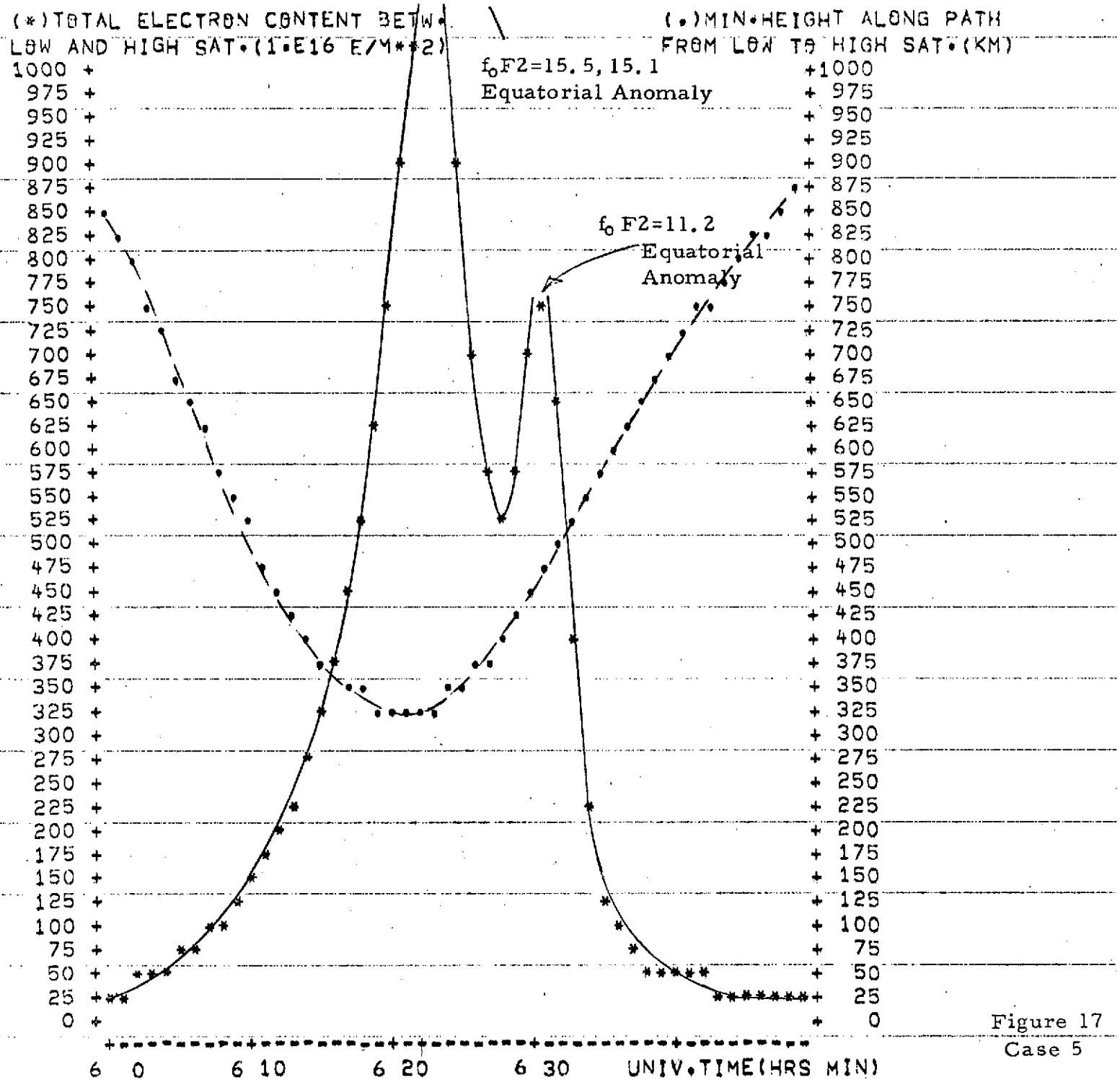

Figure 17
Case 5

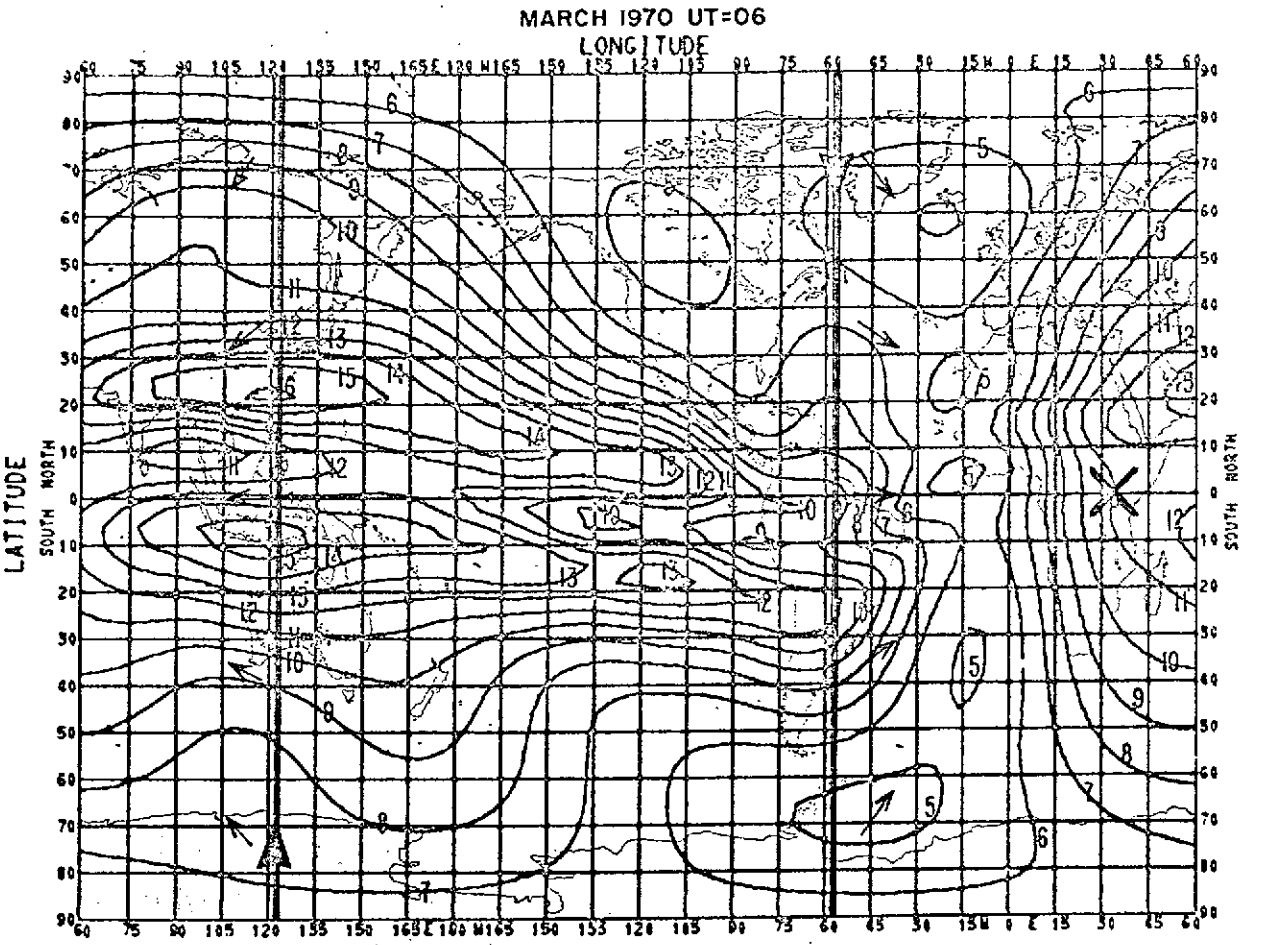

Figure 18

Case 6: Predicted global status of the monthly median f_xF2 showing the stationary high satellite position (X) and the low satellite polar orbit (→) at 200 km.

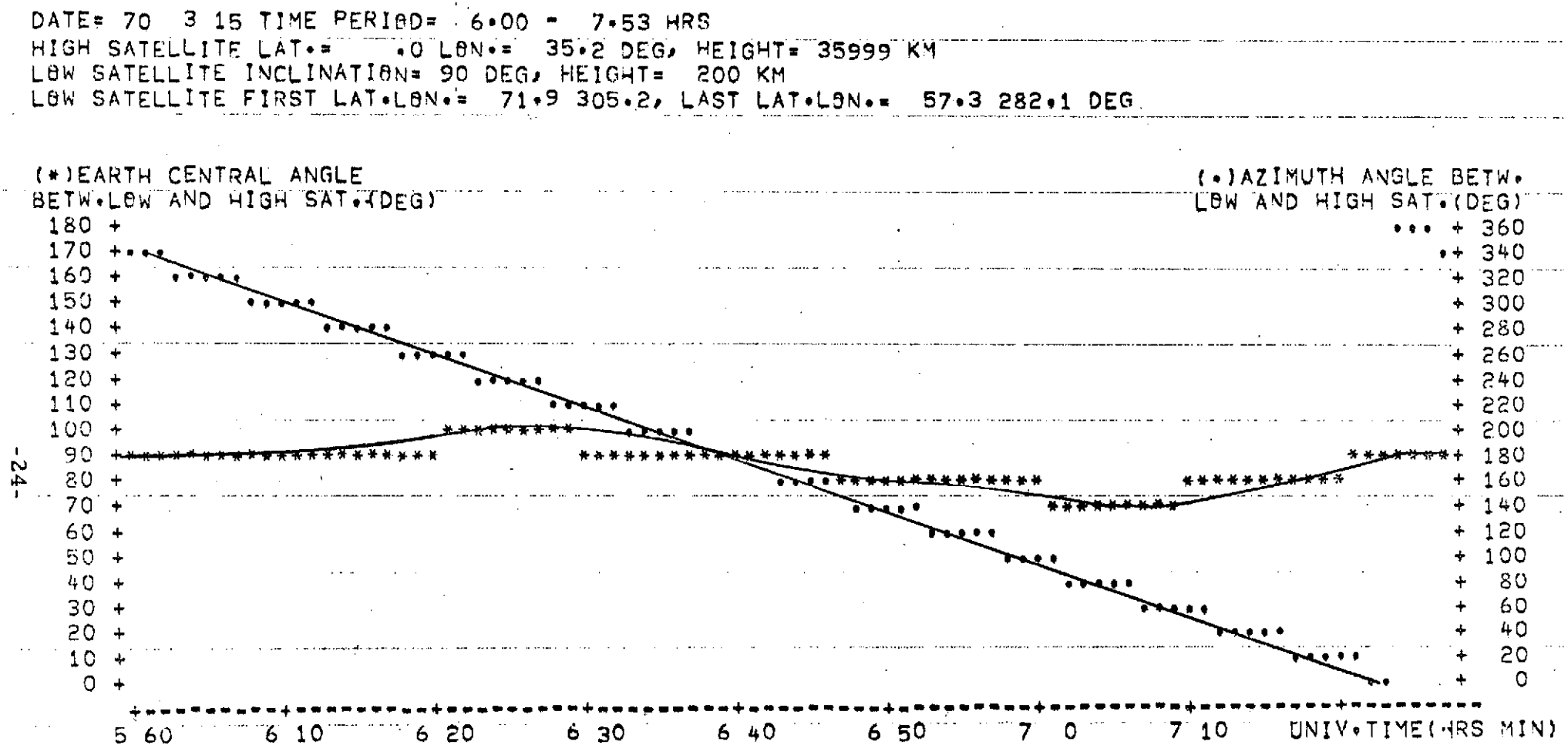

Figure 19

Case 6

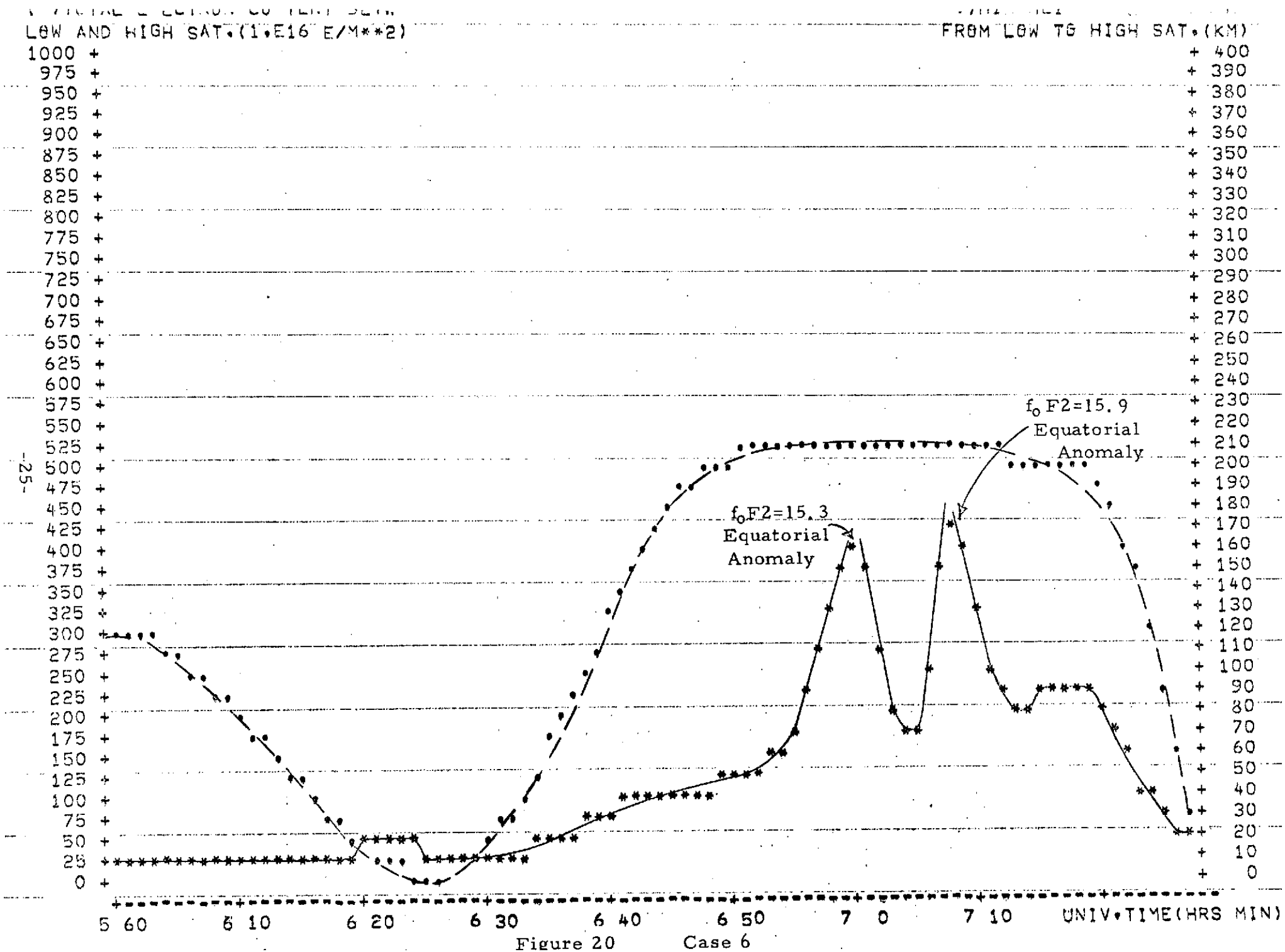

Figure 20 Case 6

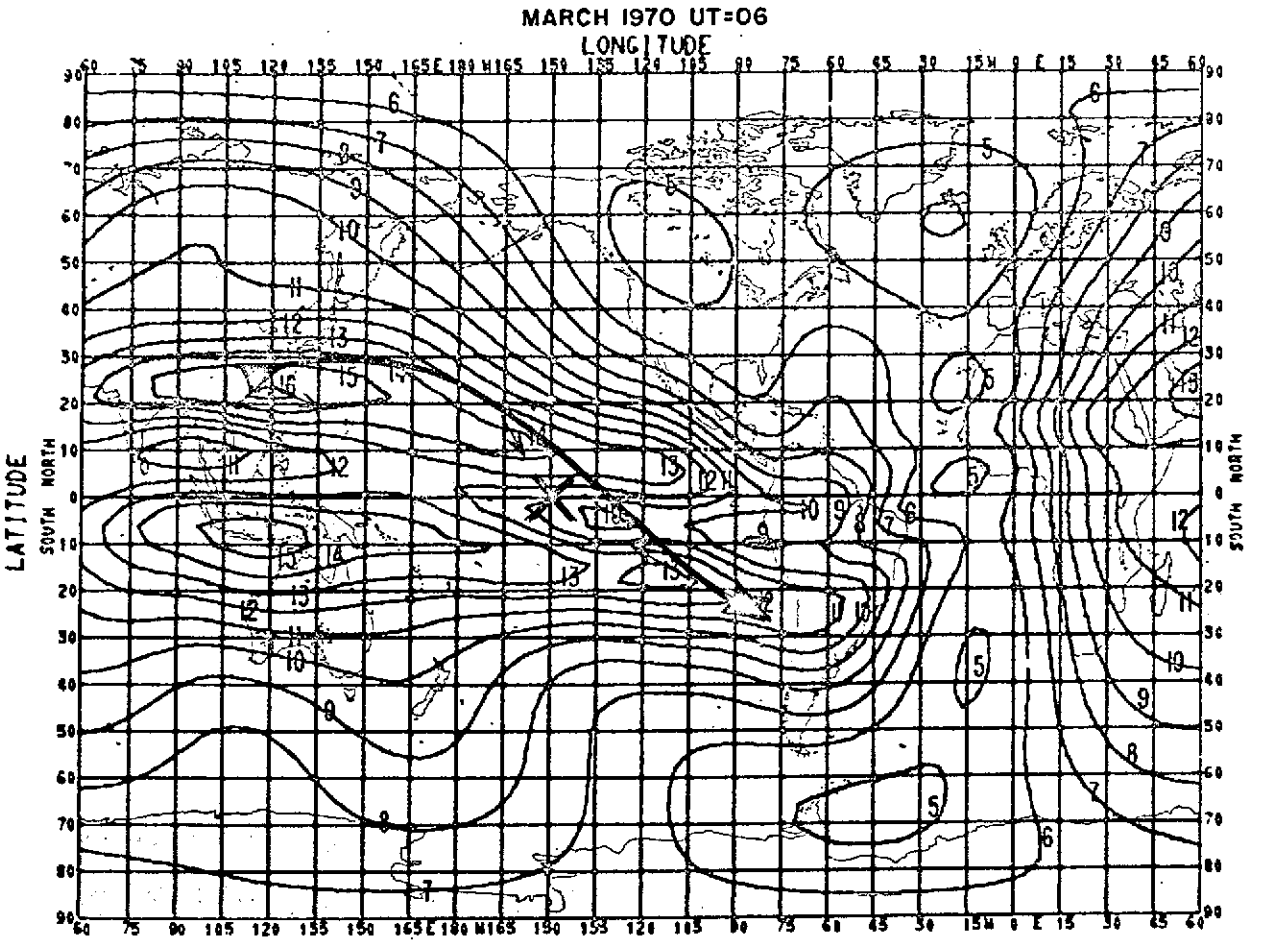

Figure 21

Case 7: Predicted global status of the monthly median f_x F2 showing the stationary high satellite position (X) and the low satellite 30 degree inclination orbit (→) at 350 km.

DATE= 70 3 15 TIME PERIOD= 6.00 - 7.32 HRS
HIGH SATELLITE LAT.= .0 LON.= 211.0 DEG, HEIGHT= 35999 KM
LOW SATELLITE INCLINATION= 30 DEG, HEIGHT= 350 KM
LOW SATELLITE FIRST LAT.LON.= 25.5 112.7, LAST LAT.LON.= 5.7 46.6 DEG

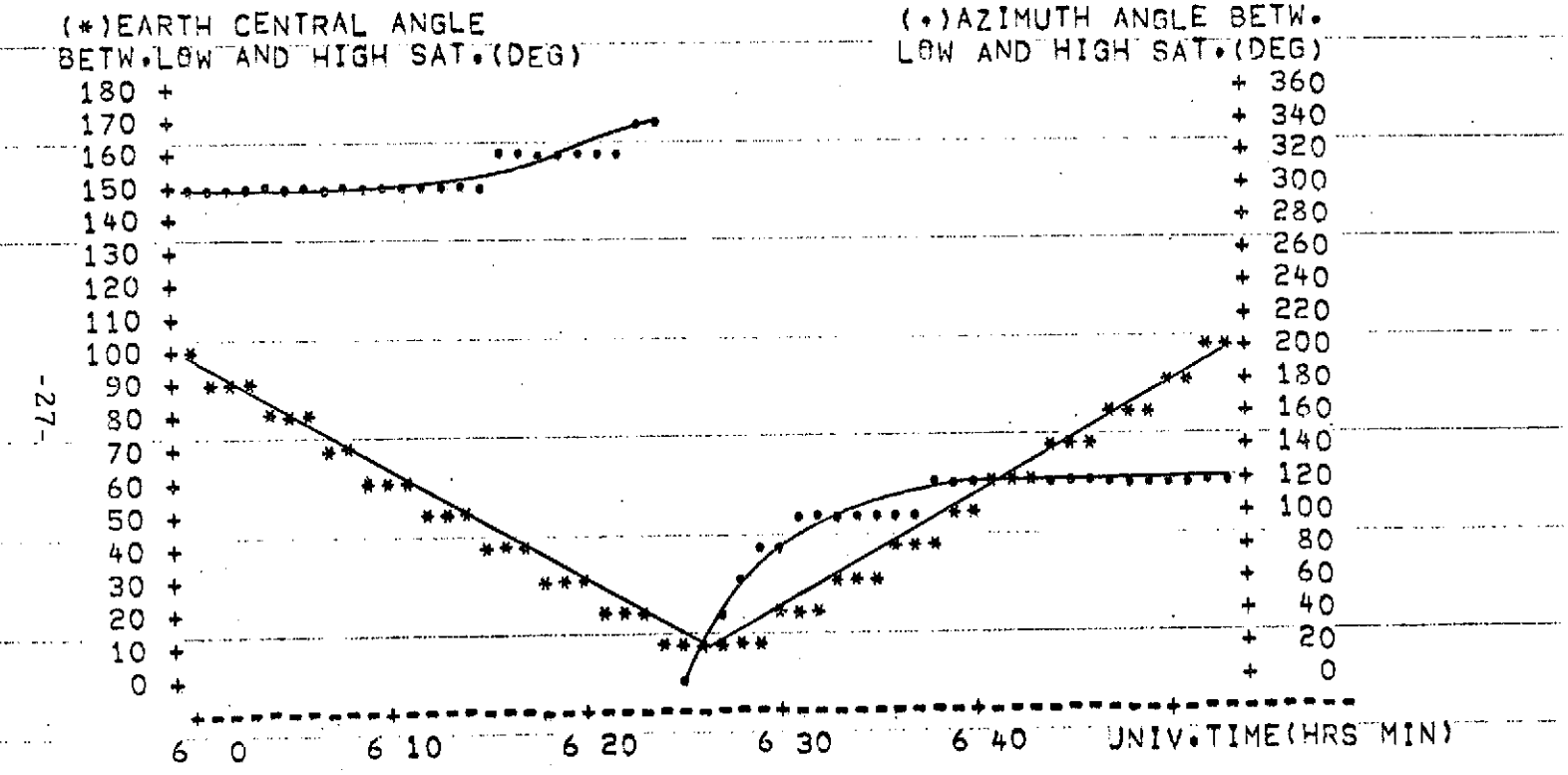

Figure 22

Case 7

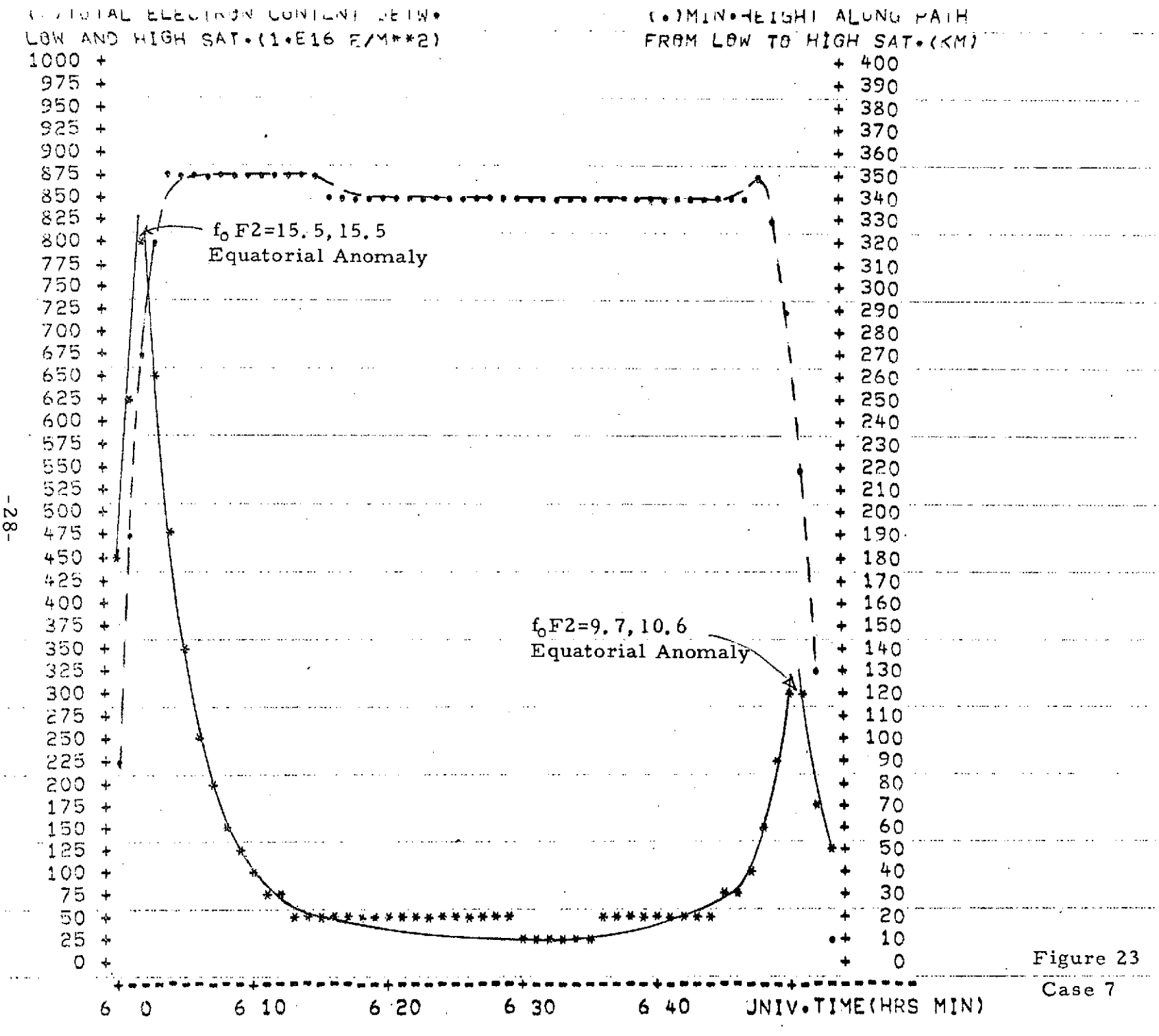

Figure 23
Case 7

Table 1.

CONVERSION TABLE

Electron Content (10^{16} e/m^2)	versus	Range Correction (meters)
0		0
25		514
50		1028
75		1542
100		2056
125		2570
150		3084
175		3598
200		4112
225		4626
250		5140
275		5654
300		6168
325		6682
350		7196
375		7710
400		8224
425		8739
450		9253
475		9767
500		10281
525		10795
550		11309
575		11823
600		12337
625		12851
650		13365
675		13879
700		14393
725		14907
750		15421
775		15935
800		16449
825		16963
850		17477
875		17991
900		18505
925		19019
950		19533
975		20047
1000		20561

3.0 RANGE RATE CORRECTIONS

A problem can occur in computing range rate corrections through the ionosphere to a satellite. Many Doppler satellite tracking systems integrate cycle counts over a few seconds of time. The ionospheric corrections for such a technique are best obtained by range differencing the ionospheric corrections and dividing by the integration period; hence time, elevation and azimuth changes are incorporated. A typical ionospheric range rate correction can be significantly changed by the sixth digit in the ionospheric range correction; precautions have therefore to be taken to ensure that no irregularities occur in computing the two adjacent range corrections. Furthermore, the ionospheric height at the ray intersection point must be computed to 1 km convergence in order to obtain a precise ionospheric latitude and longitude for f_0F2 computations. An error of over 1 km in h_mF2 will cause the f_0F2 value to be very slightly different,and from this a change in the 5th or 6th digit in range can easily arise leading to very large errors in range rate. It is not claimed that h_mF2 has to be accurate to 1 km as this is an impossible prediction, but the values of h_mF2 should be consistent in their calculation to 1 km convergence.

The theoretical approach to range rate correction either by differentiating range or using the deviation angle of arrival at the satellite is in no way accurate. The differentiating technique yields a correction to an instantaneous measurement which can vary greatly from the correction to Doppler range rate measured over a finite time interval, from a fraction of a second up to over a minute's time. In addition, the range rate correction is not only influenced by the change in the satellite position, but also by the changing ionosphere below the moving satellite, which has mostly been neglected in either approach. To explain this fact, consider the range correction ΔR as given by

$$\Delta R = \frac{KN_I}{\sin E} \qquad \text{where } K = \frac{40.3}{f^2},$$

N_T is the integrated vertical content and E is the local elevation angle in the ionosphere. Differentiating ΔR while considering the case where the satellite passes directly overhead where no azimuth change is observed:

$$\dot{\Delta R} = -KN_T \frac{\cos E}{\sin^2 E} \dot{E} + \frac{K}{\sin E} \underset{t=\text{constant}}{\frac{\delta N_I}{\delta E}} \dot{E} + \frac{K}{\sin E} \underset{E=\text{constant}}{\frac{\delta N_T}{\delta t}} \qquad (1)$$

In this equation the first term is in many cases the only one used, but it applies only to the instantaneous change in the satellite position. The other two terms are, however, often dominant. The second term is due to the positional change in the ionosphere and the last term represents the time variation of the ionosphere. For instance, with a high satellite moving east-west across the north-south ionospheric gradients at sunrise, the time variation is dominant as these gradients move towards the west with time. For a satellite moving north-south across the east-west ionospheric gradients near the equator, the time variation in the ionosphere is very small because the gradients change little in position while the ionosphere rotates with time. The second term which indicates positional change in the ionosphere is dominant for lower satellites where the ray path to the observer moves faster through the ionosphere. In cases where the satellite does not pass overhead, the azimuth change must also be considered.

In order to examine the relative importance of the three components of the range rate correction in (1), two computerized orbit simulations were performed. The first simulation generated range and range rate corrections for a station near the equator at 218 degrees east longitude (Station A) at a time when the tracking by that station would be heavily affected by the equatorial anomaly. The orbits generated for Station A passed directly overhead with inclination 90 degrees at heights of 500, 1000, and 10^{10} kilometers. The second simulation generated corrections for a tracking station located on the equator (Station B) at 355 degrees east longitude at a time when tracking would be heavily affected by the sunrise effect. The orbits generated for this station passed directly overhead

at an inclination of 0 degrees at heights of 500, 1000, and 10^{10} kilometers. Figure 24 illustrates the locations of the two stations. For each orbit, range rate corrections were generated by differencing range corrections at 1/4, 1/2, 1, 10, and 30 second intervals. An instantaneous range rate correction, computed by just differentiating the range instantaneously, was also calculated to investigate the possibility of its use as an approximation of the range rate correction as opposed to range differencing. By looking at Figures 25 and 26 one can see that the instantaneous range rate is not a good approximation, implying that the positional change in the ionosphere and the time change of the ionosphere can be dominant.

Figures 27 through 34 are plots of the percentages of the range rate correction that are due to the three components in equation (1). The data plotted are for Station A and B at satellite heights of 500 kilometers and 10^{10} kilometers and with range differencing done at 1/4 and 30 second intervals. An illustration of the effect of time variation on range rate corrections may be observed by examining the component due to ionospheric time change plotted in the above figures. The time change component is small for Station A and large for Station B, particularly for the high altitude orbit. This may be explained by studying the figure of ionospheric gradients (Figure 24). As Station A moves east under the ionosphere, there will be little change in the gradients. For Station B, however, the movement of the earth under the ionosphere results in a considerable change in the ionospheric gradients. A close study of the graphs will also indicate that for a low orbiting satellite the positional change is dominant where the ionospheric gradients are large.

In order to investigate the accuracies of numerical integration of total content which must be used for the range differencing approach to range rate, we can carry out some tests integrating vertically through the ionosphere and comparing the results with the theoretical closed form solution. Figure 35 is a plot of the magnitude of error incurred in using

numerical integration techniques to estimate the integrated electron content. The solid and dotted lines represent the error in using the trapezoidal rule for integration with .5 and 1 kilometer step sizes. The dashed and dotted-dashed lines represent the error in using Simpson's rule for numerical integration up to (h_m+d) and the trapezoidal rule thereafter. (h_m+d) is the point on the profile where the parabolic portion of the curve meets the exponential portion. The .5 and 1 kilometer step sizes were also used for this integration. Also sketched on the plots are the ionospheric profiles to which the reader may refer in interpreting the plots. By inspecting the two plots, one may see that there is a large spike in the curve at the bottom of the profile. There are also large errors near the height of the maximum electron density, h_m, and at the separations between the exponential layers. The error between the exponential layers may be eliminated to a great extent by excluding these points from the integration process. The use of Simpson's rule eliminates most of the error in the biparabolic and parabolic layers except for the first step in the biparabolic region and at h_m. The points near h_m may also be eliminated from the integration, but the bottom of the profile poses a more difficult problem.

When the trapezoidal rule is used for integration, the errors in the bottom of the profile balance the errors in the top of the profile because of a difference in signs. If, however, the integration had been started at a slightly higher altitude, the error in the total electron content would have been much larger. Table 1 illustrates the increase in error in total electron content when the numerical integration is started at successively higher altitudes.

Step sizes like .5 and 1 kilometer are impractical in application, however, since the calculations which must be done to compute f_0F2 require a significant amount of computer time and must be performed for each step.

Several tests similar to those just described were run to compare the accuracies of different types of numerical integration techniques to evaluate electron content between a stationery high satellite and a low satellite. The high satellite was placed at 1000 kilometers. The low satellite was placed directly underneath the high satellite under the ionosphere at 200 km. Various step sizes were chosen at which to evaluate the electron densities which were then integrated to calculate electron content. Table 2 contains a summary of the results of these tests.

The Mariner Mars satellite needs an accuracy of 6 or 7 digits in the range correction in order to get the necessary accuracy for range rate by differencing. Since ΔR is directly porportional to electron content by the equation,

$$\Delta R = \frac{40.3 \times N_I}{f^2} ,$$

the electron content must be consistent to the 6th or 7th digit to achieve the necessary accuracy in ΔR. In every case in Table 2 where the electron content is consistent to 6 or 7 digits, the step size is at most 2.5 kilometers. The use of such a step size, however, is not practical. The most accurate results appear to be obtained by using the trapezoidal rule with .5 and 1.0 kilometer step sizes. We have already discussed the fact that these results are misleading since errors in the exponential portion of the profile are cancelled by errors in the biparabolic portion of the profile. In addition, if integration had been started 10 or 20 kilometers higher, the results for the 1 kilometer step size would not have had 6 significant digits of accuracy.

More accurate methods of numerical integration which can be used with a larger step size need to be found or developed through future study. The studies discussed here have all been vertically through an ionosphere with a parabolic or exponential profile. In reality the line of sight between the two satellites in question will have an electron density profile totally

different from the simple forms discussed making the selection of the integrating mechanism much more difficult.

The problems in numerical integration accuracy pose a great problem in the computation of range rate by range differencing in a TDRS system. If the non-stationary satellite is being tracked near to the horizon of the earth, then very rapid and enormous changes in total electron content along the ray path are evident at certain times and places. The computation of this total electron content by numerical integration to give the accuracy one needs is a major problem. The ionosphere model, of course, gives the correct values of electron density; but the choice of an accurate step size for integration may make the time required to compute the required range too large for real time systems. Further research is therefore needed into the integration problems and accuracies required.

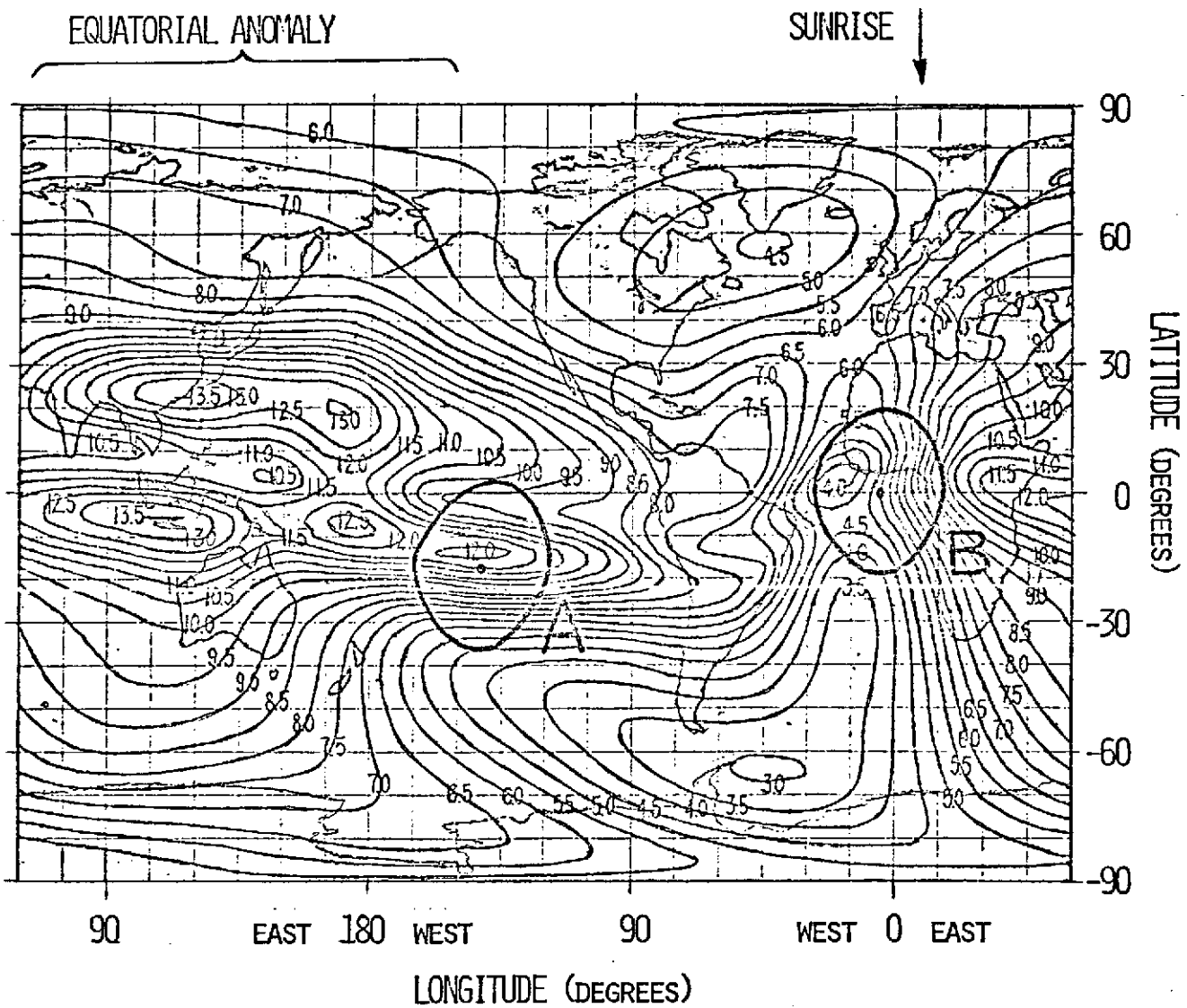

Figure 24. The predicted global status of a monthly median f_xF2 at 6.0 a.m. UT August 1968 showing areas of visibility for two hypothetical ground stations.

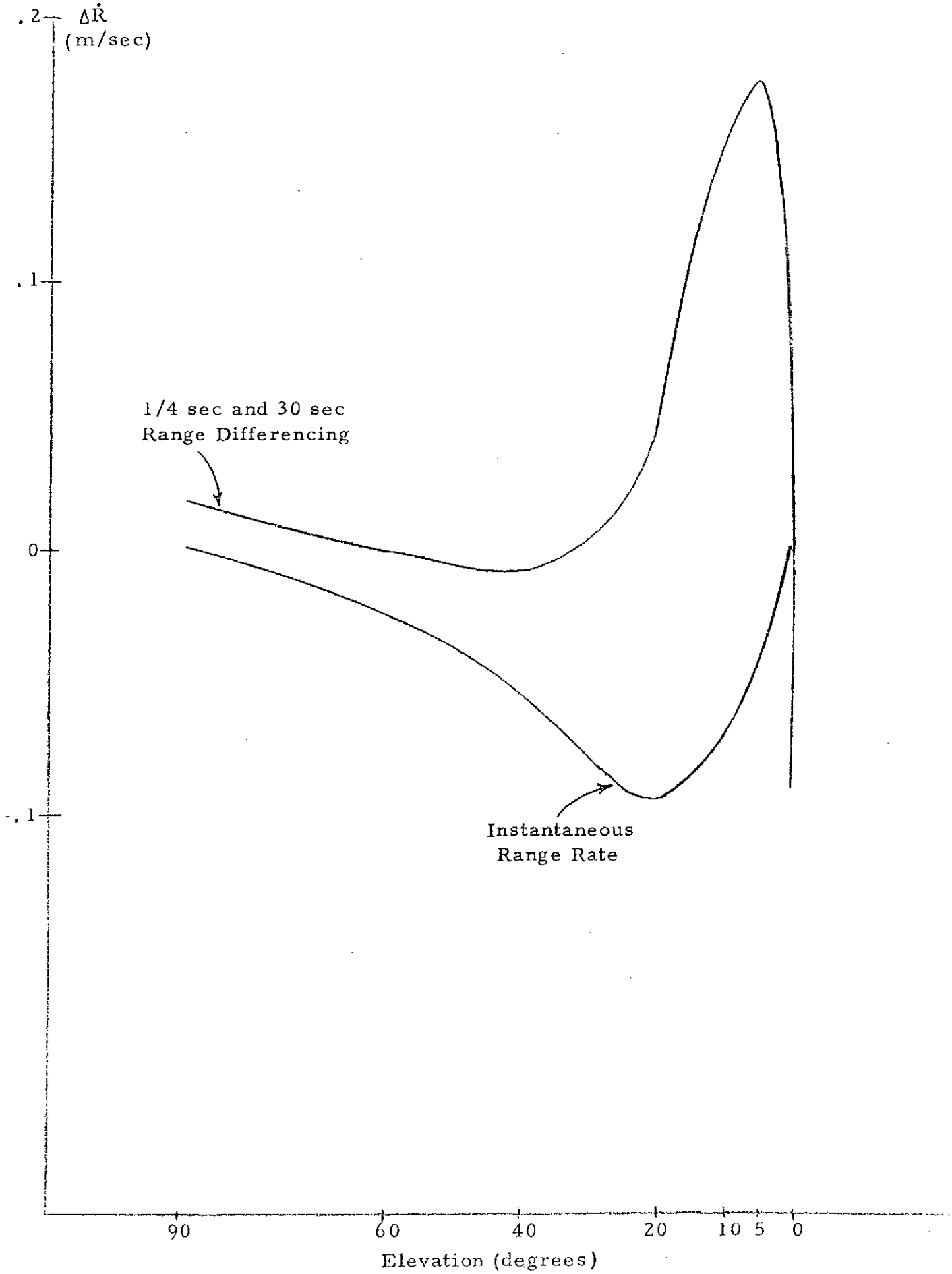

Figure 25. High Satellite (10^{4} °km) Station A

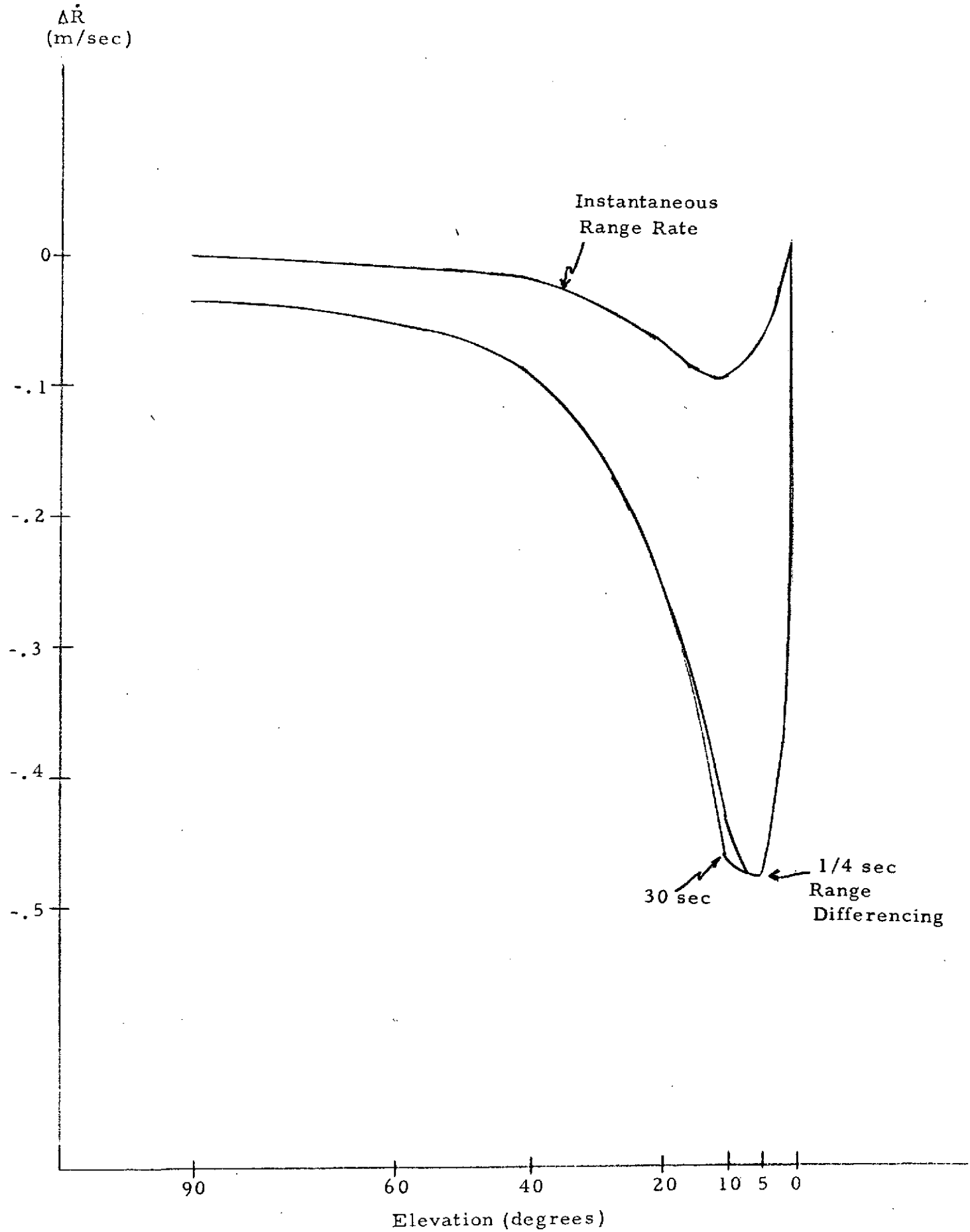

Figure 26 High Satellite (10^{10} km) Station B

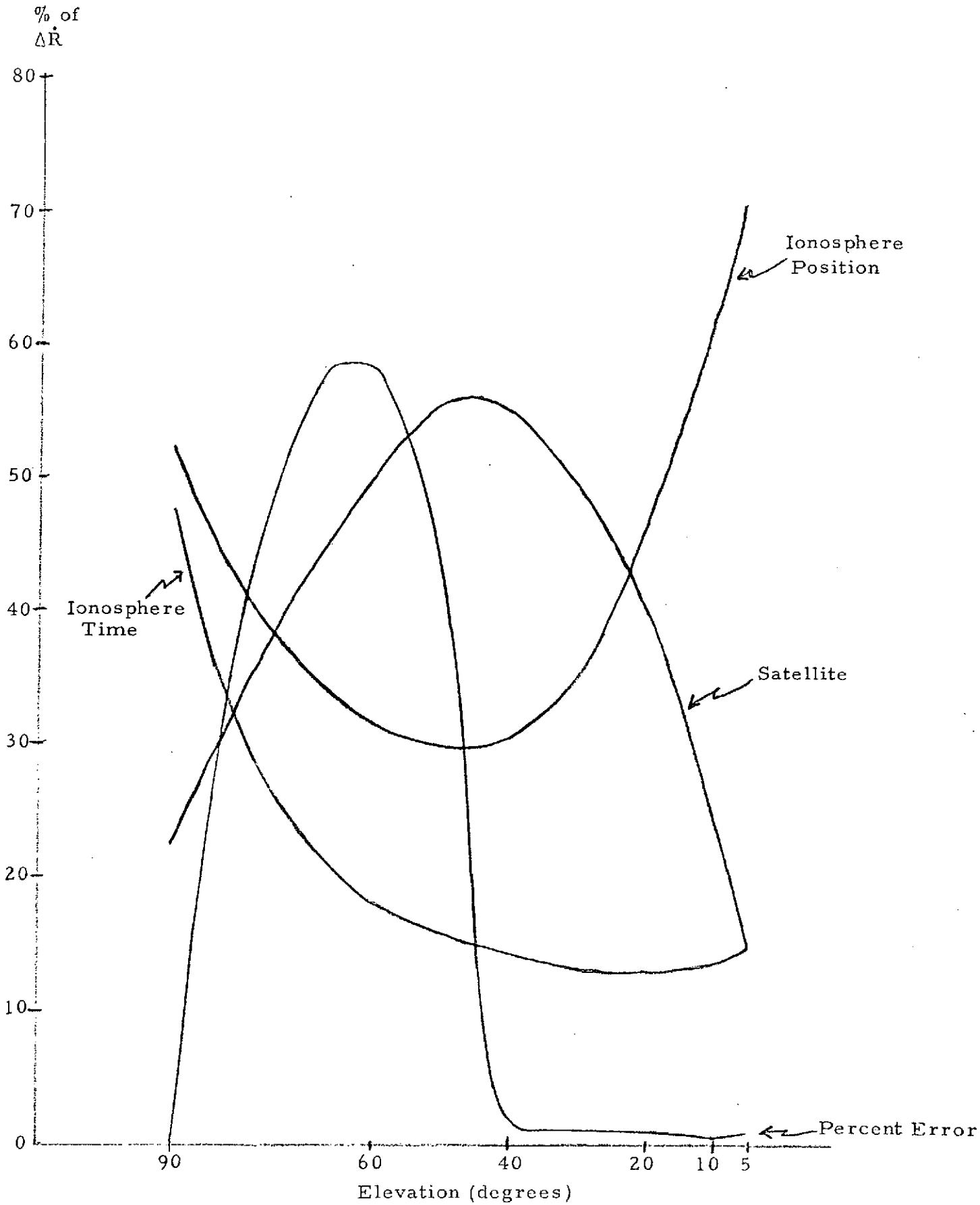

Figure 27. High Satellite (10^{10} km) Station A 1/4 Sec Interval

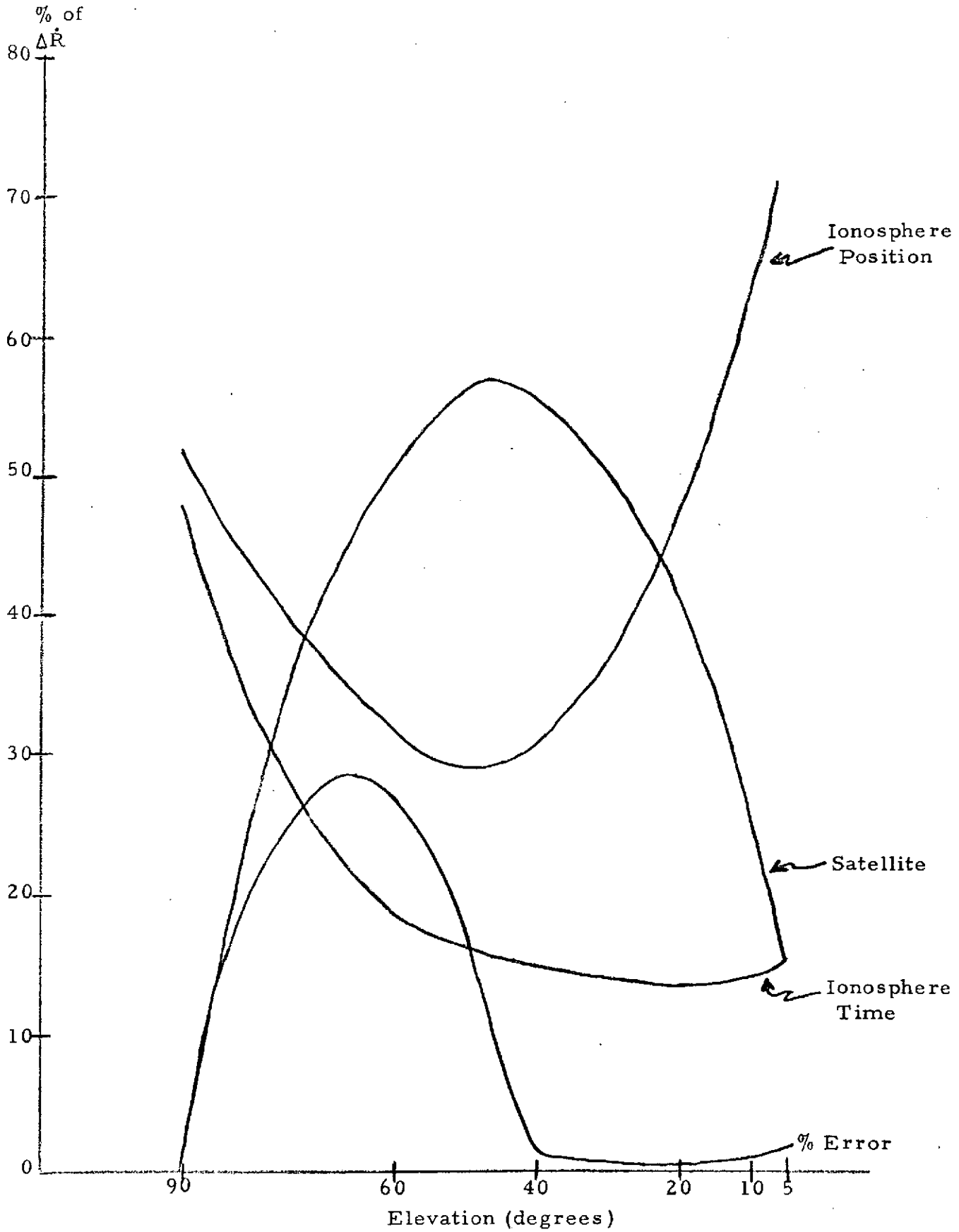

Figure 28. High Satellite (10^{10}km) Station A 30 Sec Interval

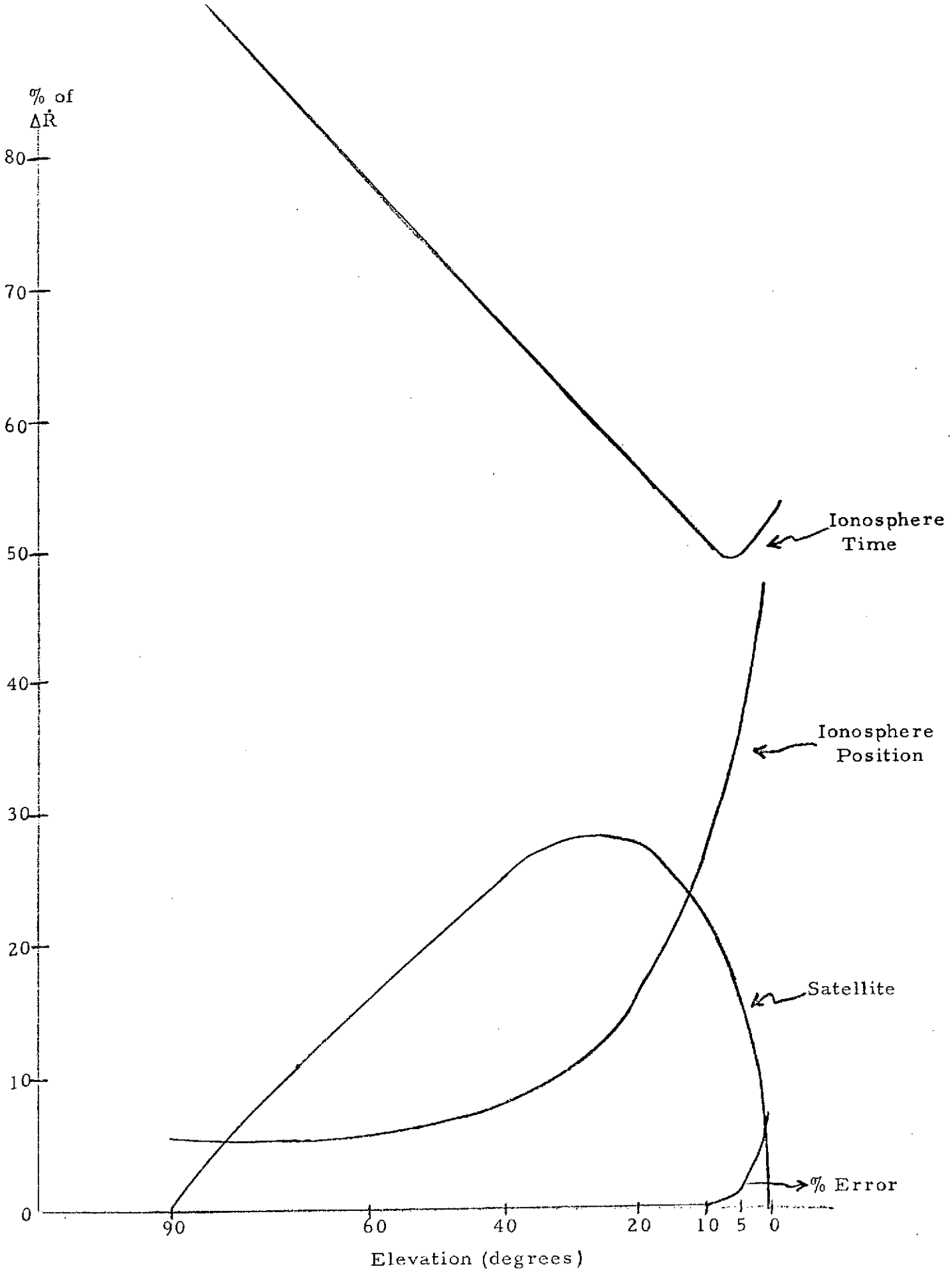

Figure 29. High Satellite (10^{10} km) Station B 1/4 Sec Interval

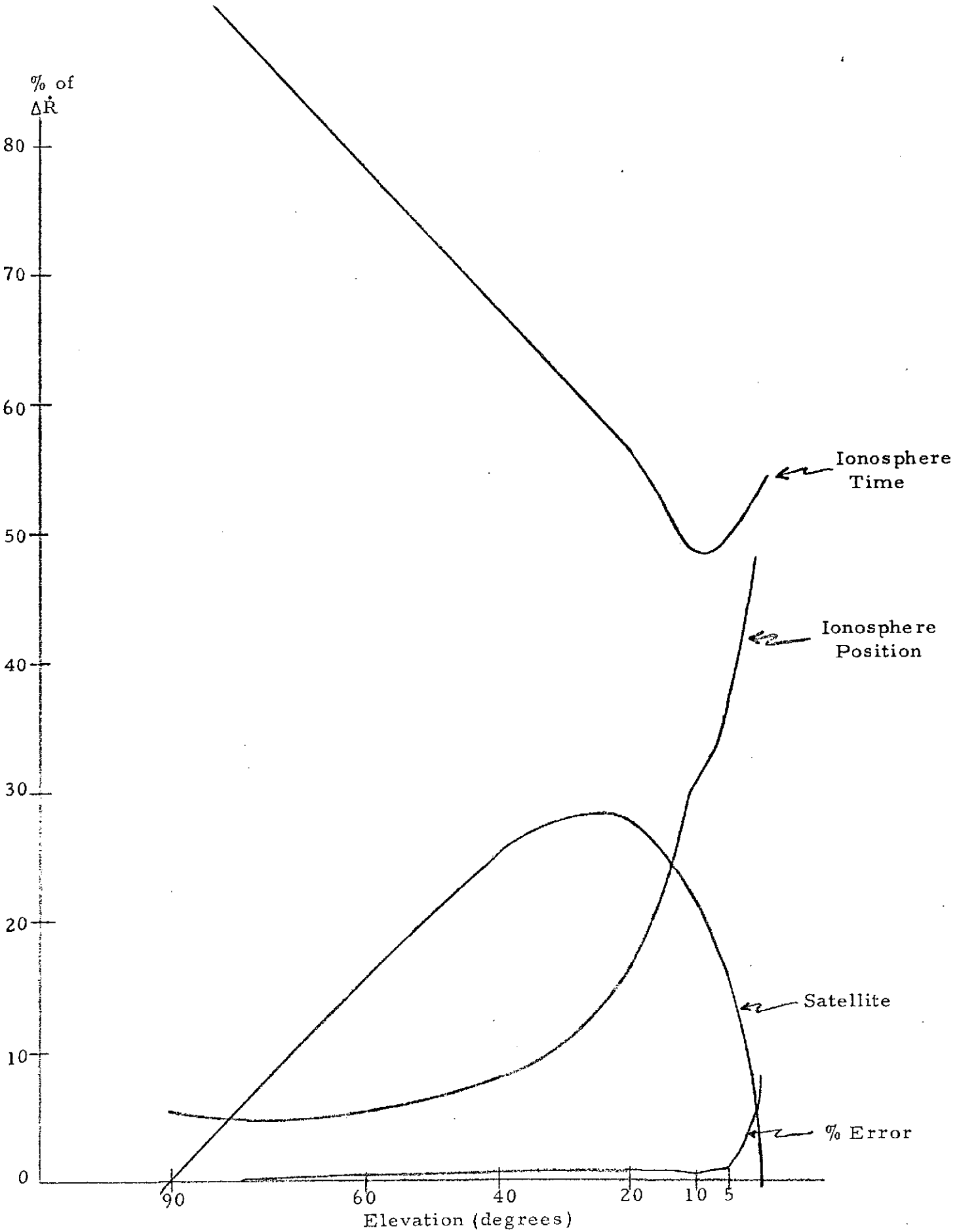

Figure 30. High Satellite (10^{1} °km) Station B 30 Sec Interval

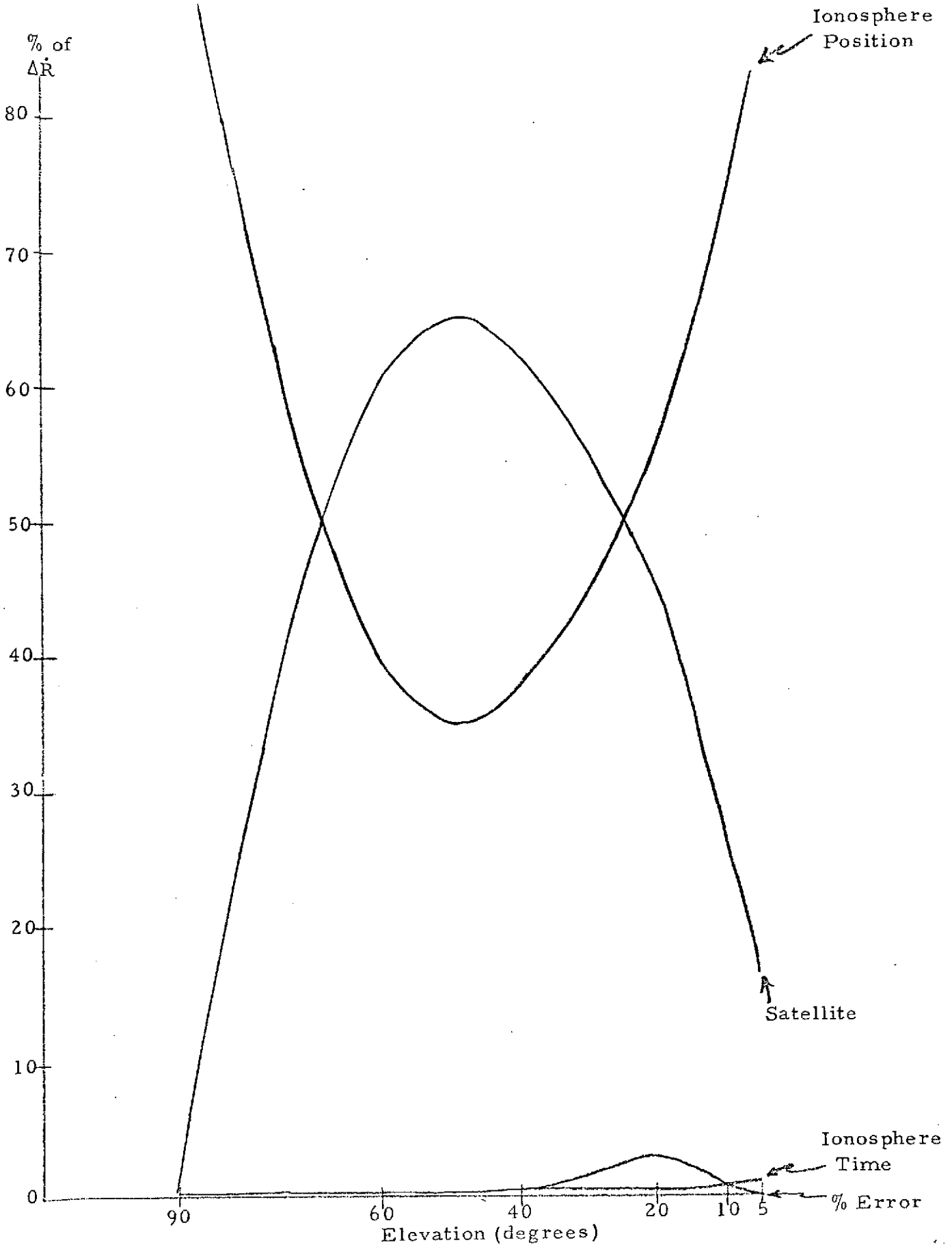

Figure 31. High Satellite (500 km) Station A 1/4 Sec Interval

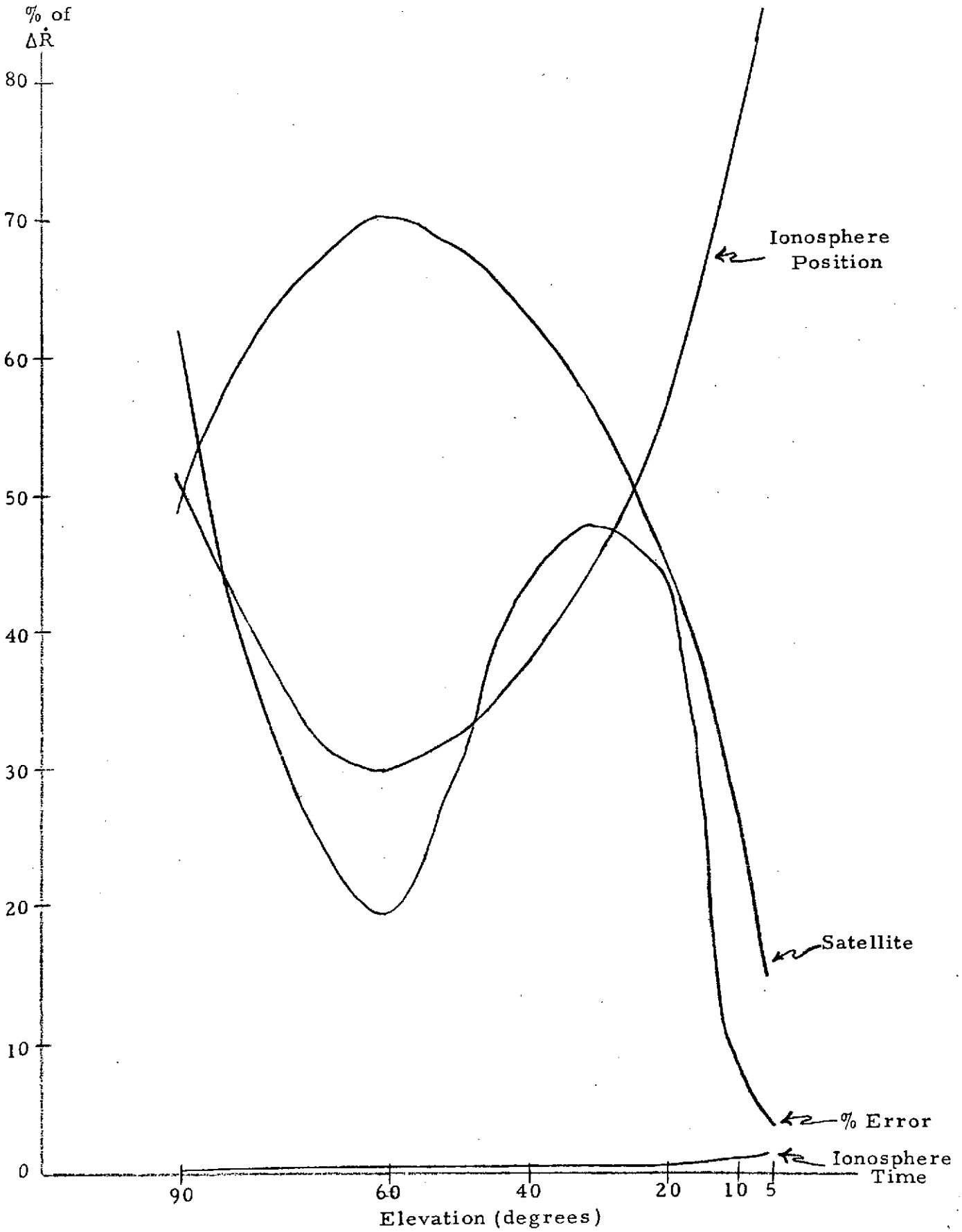

Figure 32. High Satellite (500 km) Station A 30 Sec Interval

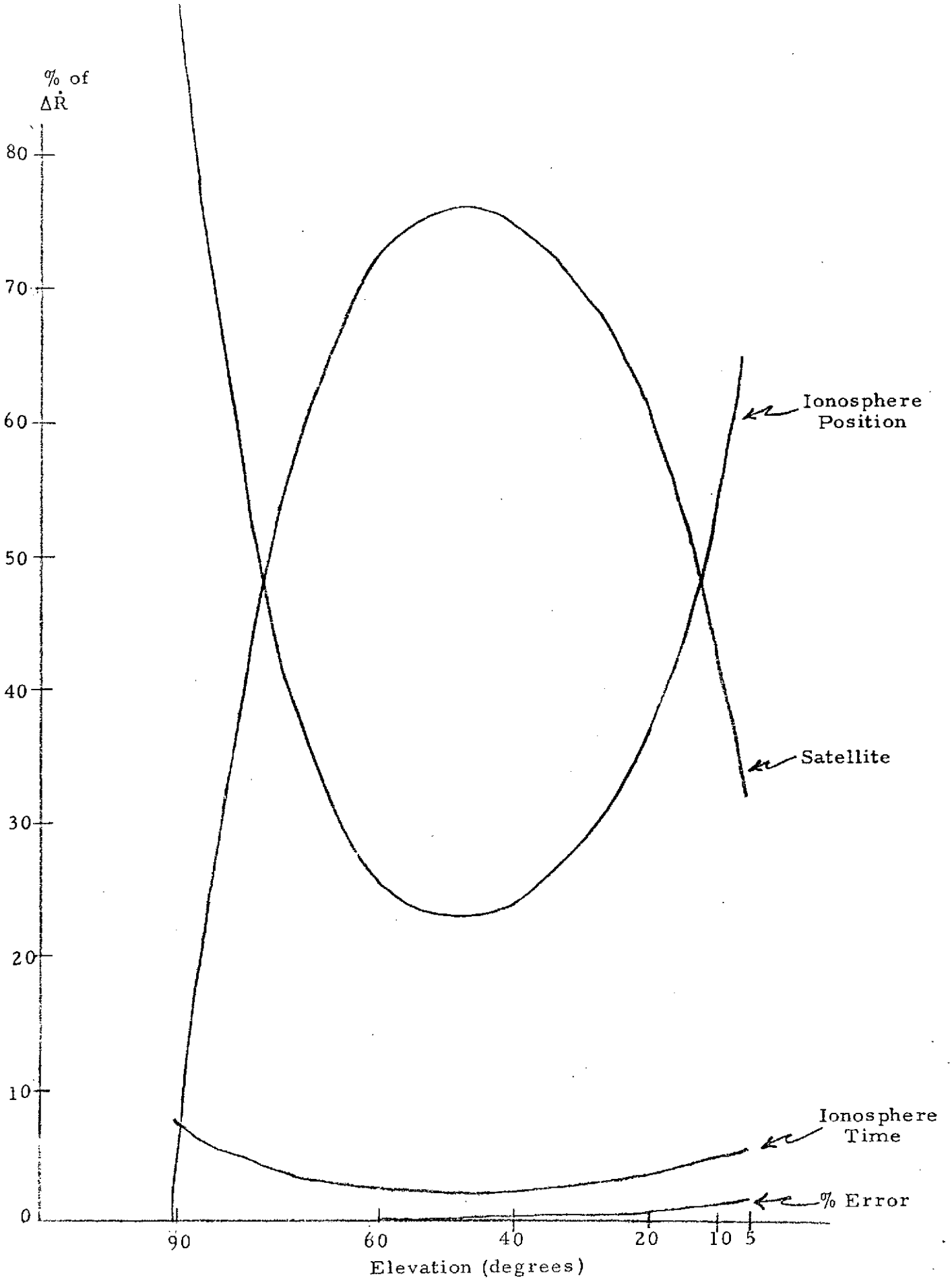

Figure 33. High Satellite (500 km) Station B 1/4 Sec Interval

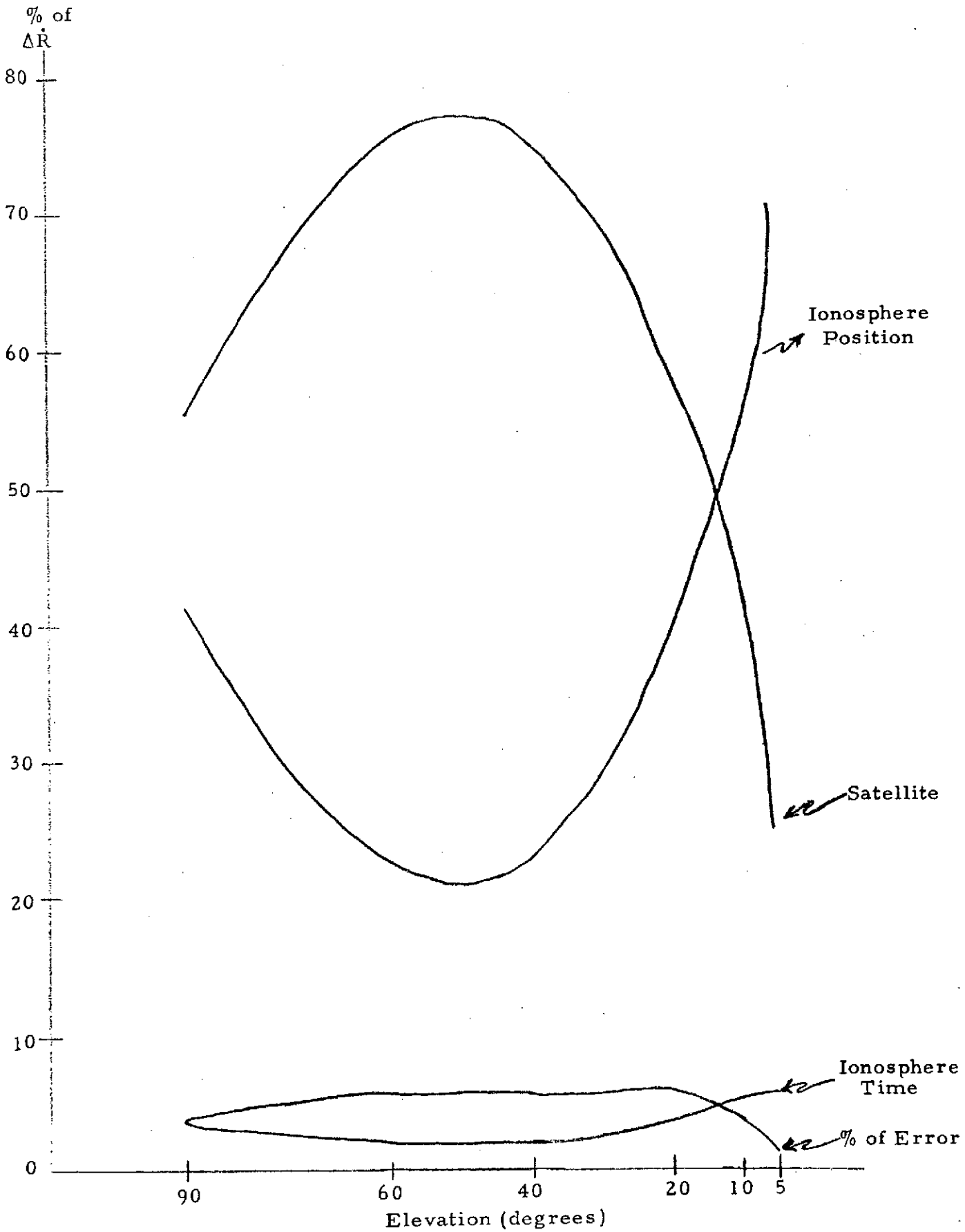

Figure 34. High Satellite (500 km) Station B 30 Sec Interval

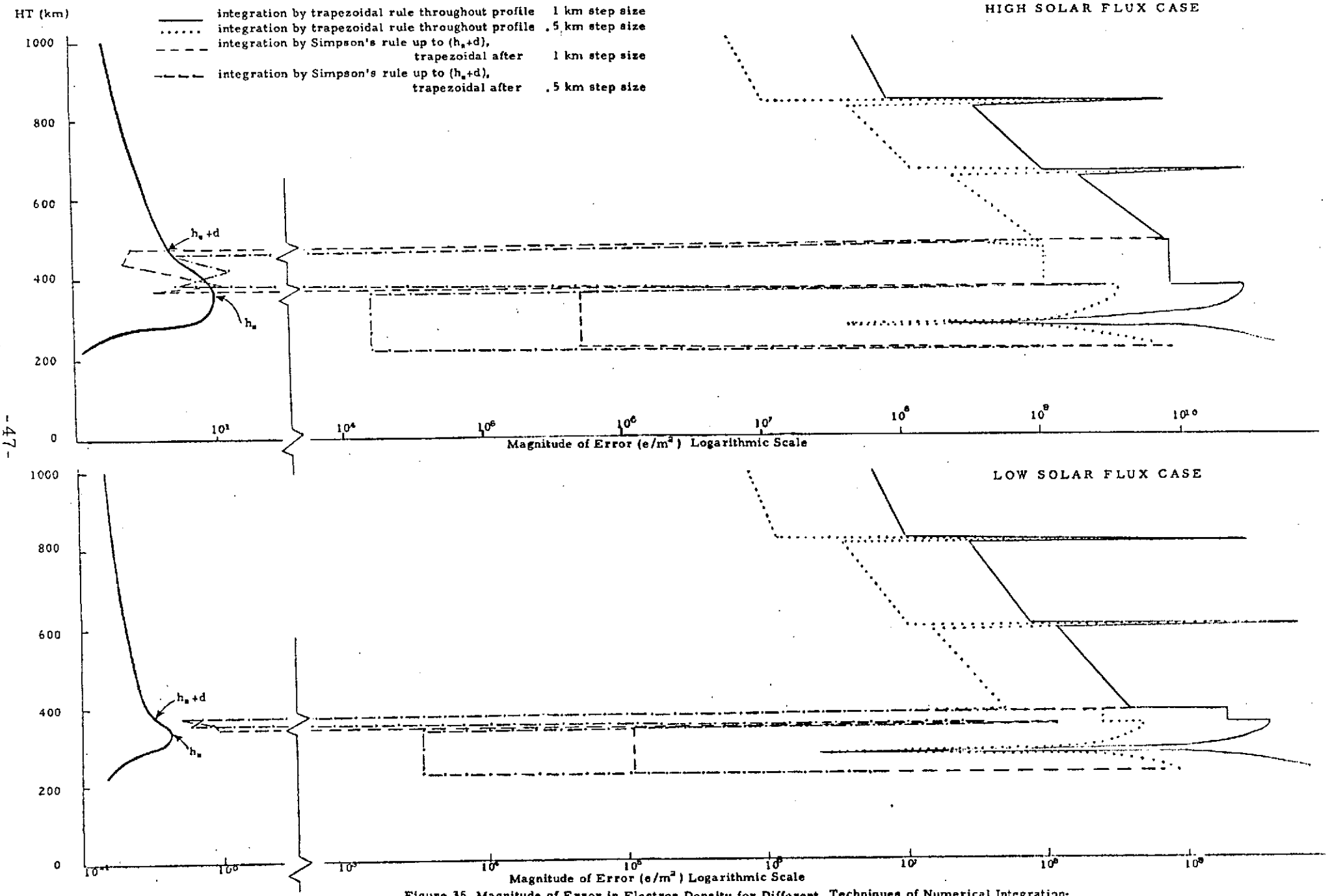

Figure 35 Magnitude of Error in Electron Density for Different Techniques of Numerical Integration

Table 2. Height of Satellite=1000 km, f_0F2=12.8180, h_m=361.382 km

Height of Start of Integration (km)	Step Size (km)	Error (electrons/m^2)
212	.5	.57032 E10
222	.5	.12488 E12
232	.5	.23644 E12
242	.5	.32160 E12
252	.5	.38236 E12
262	.5	.42075 E12
212	1.0	.42537 E11
222	1.0	.52566 E12
232	1.0	.97189 E12
242	1.0	.13125 E13
252	1.0	.15556 E13
262	1.0	.17091 E13

Table 3.

Type of Numerical Integration	Solar Flux	Step Size (km)	Closed Form Integration (el/m^2)	Numerical Integration (el/m^2)
Trapezoidal	242.0	.5	.53796147 E18	.53796147 E18*
Trapezoidal	242.0	1.0	.53796147 E18	.53796143 E18*
Trapezoidal	90.0	.5	.43989871 E17	.43989871 E17*
Trapezoidal	90.0	1.0	.43989871 E17	.43989871 E17*
Parabolic Fit Below (h_m+d), Trapezoidal Fit Above	242.0	.5	.53796147 E18	.53796171 E18*
Parabolic Fit Below (h_m+d), Trapezoidal Fit Above	242.0	1.0	.53796147 E18	.53796241 E18*
Parabolic Fit Below (h_m+d), Trapezoidal Fit Above	242.0	2.5	.53796147 E18	.53796685 E18
Parabolic Fit Below (h_m+d), Trapezoidal Fit Above	90.0	.5	.43989871 E17	.43989888 E17*
Parabolic Fit Below (h_m+d), Trapezoidal Fit Above	90.0	1.0	.43989871 E17	.43989942 E17
Parabolic Fit Below (h_m+d), Trapezoidal Fit Above	90.0	2.5	.43989871 E17	.43990256 E17

* Accurate to at least 6 significant digits

Table 3.(continued)

Type of Numerical Integration	Solar Flux	Step Size (km)		Closed Form Integration (el/m^2)	Numerical Integration (el/m^2)
		Height of low sat. 0-(h_m+d) kilometers	Height of low sat. (h_m+d)-top of profile		
Trapezoidal	242.0	.5	2.5	.53796147 E18	.53796433 E18*
Trapezoidal	242.0	1.	5.	.53796147 E18	.53797409 E18
Trapezoidal	242.0	2.	10	.53796147 E18	.53800839 E18
Trapezoidal	242.0	10.	50.	.53796147 E18	.53907553 E18
Trapezoidal	90.0	.5	2.5	.43989871 E17	.43990019 E17
Trapezoidal	90.0	1.	5.	.43989871 E17	.43990434 E17
Trapezoidal	90.0	2.	10.	.43989871 E17	.43991882 E17
Trapezoidal	90.0	10.	50.	.43989871 E17	.44043096 E17
Parabolic	242.0	.5	2.5	.53796147 E18	.53796107 E18*
Parabolic	242.0	1.	5.	.53796147 E18	.53796266 E18
Parabolic	242.0	2.	10.	.53796147 E18	.53839116 E18
Parabolic	242.0	10.	50.	.53796147 E18	.54011454 E18
Parabolic	90.0	.5	2.5	.43989871 E17	.43989880 E17*
Parabolic	90.0	1.	5.	.43989871 E17	.43989952 E17*
Parabolic	90.0	2.	10.	.43989871 E17	.44071179 E17
Parabolic	90.0	10.	50.	.43989871 E17	.44358091 E17

*Accurate to at least 6 significant digits